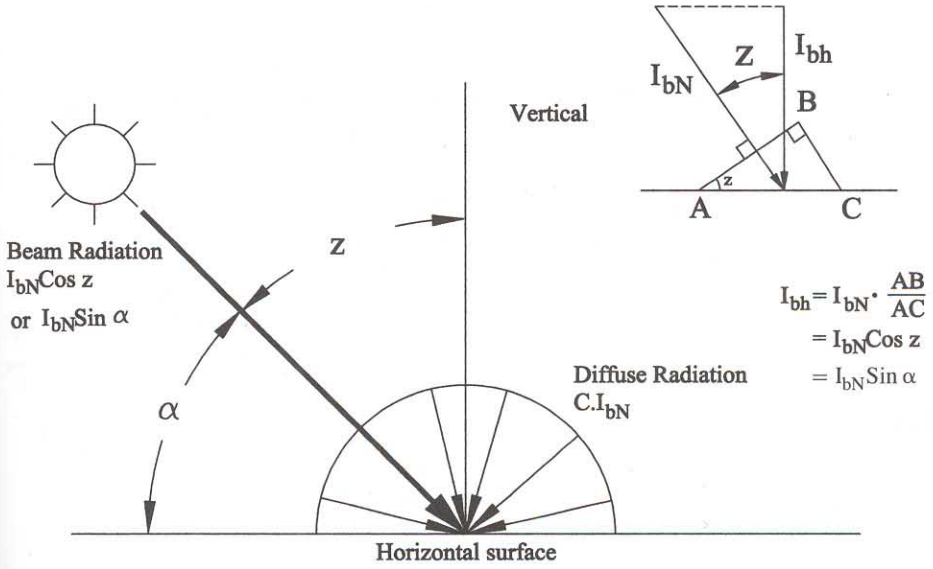

Figure 2.18. Solar radiation on a horizontal surface.

2.5.3 Solar Radiation on a Tilted Surface

Solar radiation on an arbitrary tilted surface having a tilt angle of β from the horizontal and an azimuth angle of a_w (assumed + west of south), as shown in Fig. 2.19, is the sum of components consisting of beam ($I_{b,c}$), sky diffuse ($I_{d,c}$) and ground reflected solar radiation ($I_{r,c}$):

$$I_c = I_{b,c} + I_{d,c} + I_{r,c}. \tag{2.42}$$

If i is the ***angle of incidence*** of the beam radiation on the tilted surface, it is simple to show that the instantaneous beam radiation on the surface per unit area is:

$$I_{b,c} = I_{b,N} \cos i. \tag{2.43}$$

From the geometry in Fig. 2.19, it can be shown that the angle of incidence i for the surface (angle between the normal to the surface and a line collinear with the sun's rays) is related to the solar angles as

$$\cos i = \cos \alpha \cos (a_s - a_w) \sin \beta + \sin \alpha \cos \beta. \tag{2.44}$$

The diffuse radiation on the surface ($I_{d,c}$) can be obtained by multiplying the sky diffuse radiation on a horizontal surface by the view factor between the sky and the surface:*

*The surface has been assumed infinitely large for this view factor. See Section 2.2.3.

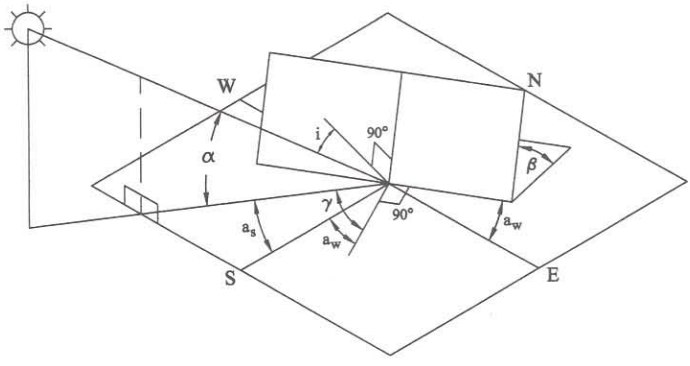

Solar Altitude Angle	α
Solar Azimuth Angle	a_s
Panel Tilt Angle	β
Panel Azimuth Angle	a_w
Incident Angle	i

Figure 2.19. Definitions of solar angles for a tilted surface.

$$\begin{aligned} I_{d,c} &= I_{d,h}(1 + \cos\beta)/2 \\ &= CI_{b,N}(1 + \cos\beta)/2 \\ &= CI_{b,N}\cos^2(\beta/2). \end{aligned} \tag{2.45}$$

The ground reflected solar radiation can be found from the total solar radiation incident on a horizontal surface and the ground reflectance ρ as:

$$I_{r,c} = I_h\rho. \tag{2.46}$$

The part of I_r intercepted by the tilted surface can be found by multiplying the ground reflected radiation by the view factor between the surface* and the ground:

$$\begin{aligned} I_{r,c} &= \rho I_h(1 - \cos\beta)/2 = \rho I_h \sin^2(\beta/2) \\ &= \rho I_{b,N}(\sin\alpha + C)\sin^2(\beta/2). \end{aligned} \tag{2.47}$$

For ordinary ground or grass, ρ is approximately 0.2 and for snow covered ground it can be taken as approximately 0.8.

Example 2.6(a). Find the instantaneous solar radiation at 12:00 noon Eastern Standard Time on a solar collector surface ($\beta = 30°$, $a_w = +10°$) on February 1 in Gainesville, FL.

Solution. From Example 2.1, for February 1:

$$n = 32,\ \delta_s = -17.5°, \text{ and } ET = -13.7 \text{ min}$$

*The tilted surface and the ground in front of it have been assumed to be infinitely large for this view factor.

For finding the values of solar radiation on the collector, we will need to calculate angles α, a_s, h_s, and i.

$$\begin{aligned}\text{Solar Time} &= LST + ET + 4(l_{st} - l_{local}) \\ &= 12{:}00 - 13.7 \text{ min} + 4(75^\circ - 82.27^\circ) \\ &= 11{:}17.2 \text{ AM},\end{aligned}$$

$$h_s = \frac{\text{minutes from solar noon}}{4 \text{ min/deg}},$$

$$= \frac{-42.8}{4} = -10.7^\circ \text{ (} - \text{before noon)}.$$

From Eq. (2.28),

$$\alpha = \sin^{-1}(\sin(29.68^\circ)\sin(-17.5^\circ) + \cos(29.68^\circ)\cos(-17.5^\circ)\cos(-10.7^\circ))$$
$$= 41.7^\circ.$$

From Eq. (2.29),

$$a_s = \sin^{-1}(\cos(-17.5^\circ)\sin(-10.7^\circ)/\cos(41.7^\circ))$$
$$= -13.7^\circ.$$

Angle of incidence i for the solar collector is given by Eq. (2.44):

$$\cos i = \cos(41.7^\circ)\cos(-13.7^\circ - 10^\circ)\sin(30^\circ) + \sin(41.7^\circ)\cos(30^\circ)$$
$$i = 23.4^\circ$$

To calculate the solar radiation using Eqs. (2.42, 2.43, 2.45, and 2.47), we need to find I_{bN} and I.

Extraterrestrial Solar Radiation

$$I = I_0[1 + 0.034\cos(360n/365.25)^\circ]$$
$$= 1353\text{W/m}^2[1 + 0.034\cos(360x32/365.25)]$$
$$= 1392\text{W/m}^2,$$
$$I_{b,N} = C_n I e^{-k/\sin\alpha}$$

(Find k from Table 2.4. Assume $C_n = 1$)

$$= 1392e^{-0.144/\sin(41.7^\circ)}$$
$$= 1121\text{W/m}^2.$$

Beam radiation on the collector (Eq. 2.43):

$$\begin{aligned} I_{b,c} &= I_{b,N} \cos i \\ &= (1121)\cos(23.4°) \\ &= 1029 \text{W/m}^2. \end{aligned}$$

Sky diffuse radiation on the collector (Eq. 2.45):

$$\begin{aligned} I_{d,c} &= C I_{b,N} \cos^2(\beta/2) \\ &= (0.060)(1121)\cos^2(30/2) \end{aligned}$$

(Find C from Table 2.4.)

$$63 \text{W/m}^2.$$

Ground reflected radiation on the collector (Eq. 2.47):

$$I_{r,c} = \rho I_{b,N}(\sin \alpha + C)\sin^2(\beta/2)$$

Assume

$$\begin{aligned} \rho &= 0.2 \\ I_{r,c} &= (0.2)(1121)(\sin 41.7° + 0.060)\sin^2(15°) \\ &= 11 \text{W/m}^2. \end{aligned}$$

Total insolation on the collector:

$$I_c = 1029 + 63 + 11 = 1103 \text{W/m}^2.$$

Example 2.6(b). Repeat the calculations in Example 2.6(a) for a north facing solar collector ($\beta = 30°$, $a_w = 10°$) in Buenos Aires, Argentina. (latitude = 34° − 35′S, longitude = 58° − 29′W, Standard Meridian = 45°W)

Solution. Following the procedure in Example 2.6(a), the solar angles and the angle of incidence are found as:

$$\begin{aligned} \text{Solar Time} &= 12{:}00 - 13.7 \text{ min} + 4(45° - 58.48°)\text{min} \\ &= 10{:}52 \text{ AM} \\ h_s &= -68/4 = -17° \end{aligned}$$

$$\begin{aligned} \alpha &= \sin^{-1}[\sin(-34.58°)\sin(-17.5°) + \cos(-34.58°)\cos(-17.5°)\cos(-17°)] \\ &= 67.2° \end{aligned}$$

$$a_s = \sin^{-1}[\cos(-17.5°)\sin(-17°)/\cos(67.2°)]$$
$$= -46°$$

Therefore, the angle of incidence

$$i = \cos^{-1}[\cos(67.2°)\cos(-46° - 10°)\sin(30°) + \sin(67.2°)\cos(30°)]$$
$$= 24.95°$$

Assuming that the solar radiation model used in Example 2.2(a) applies. (Note: the model was developed for locations in the U.S.)

$$I_{b,N} = 1392\ e^{-0.144/\sin(67.2°)}$$
$$= 1191\ W/m^2$$
$$I_{b,c} = 1191\cos(24.95°)$$
$$= 1080\ W/m^2$$
$$I_{d,c} = (0.060)(1191)\cos^2(30°/2)$$
$$= 67\ W/m^2$$
$$I_{r,c} = (0.2)(1191)(\sin 67.2° + 0.060)\sin^2(15°)$$
$$= 16\ W/m^2$$

Total insolation on the collector

$$I_c = 1080 + 67 + 16$$
$$= 1163\ W/m^2$$

2.5.4 Monthly Solar Radiation Estimation Models

One of the earliest methods of estimating solar radiation on a horizontal surface was proposed by the pioneer spectroscopist Angström. It was a simple linear model relating average horizontal radiation to clear-day radiation and to the sunshine level, that is, percent of possible hours of sunshine. Since the definition of a clear day is somewhat nebulous, Page [57] refined the method and based it on extraterrestrial radiation instead of the ill-defined clear day:

$$\overline{H}_h = \overline{H}_{o,h}\left(a + b\frac{\overline{n}}{\overline{N}}\right)$$
$$= \overline{H}_{o,h}\left(a + b\frac{\overline{PS}}{100}\right) \qquad (2.48)$$

where $\overline{H}_h$ and $\overline{H}_{o,h}$ are the horizontal terrestrial, and horizontal extraterrestrial radiation levels averaged for a month, $\overline{PS}$ is the monthly averaged percent of possible sunshine (that is, hours of sunshine/maximum possible duration of sunshine $\times$ 100), a and b are constants for a given site, and $\overline{n}$ and $\overline{N}$ are the monthly average numbers of hours of bright sunshine and day length respectively. The ratio $\overline{n}/\overline{N}$ is also equivalent to the monthly average percent sunshine ($\overline{PS}$). $\overline{H}_{o,h}$ can be calculated by finding $H_{o,h}$ from the following equation (2.49), using Eqs. (2.35) and (2.44) and averaging $I_{o,h}$ for the number of days in each month; or data in Appendix 2 (Table A2.2) can be used.

$$H_{o,h} = \int_{t_{sr}}^{t_{ss}} I \sin \alpha dt \tag{2.49}$$

Some typical values of a and b are given in Table 2.5 [46]. Additional values for worldwide locations are given in Appendix 2 (Table A2.4).

Example 2.7. Using the predictive method of Angström or Page, estimate the monthly solar radiation for the North Central Sahara Desert (Tamanrasset, Algeria area) at latitude = 25°N. Percentages of possible sunshine and extraterrestrial radiation for this site are given in the table below.

Solution. Using the climate data given, the expected monthly average horizontal radiation for the North Sahara is calculated in the following table using $a = 0.30$ and $b = 0.43$ from Table 2.5.

		$\overline{H}_{o,h}$[a]	$\overline{H}_h$	
Month	$\overline{PS}/100$	(kJ/m² · day)	kJ/m² · day	Btu/ft² · day
Jan.	0.88	23,902	16,215	1425
Feb.	0.83	28,115	18,469	1626
Mar.	0.90	32,848	22,143	1950
Apr.	0.85	37,111	24,697	2174
May	0.80	39.356	25,345	2231
June	0.76	40,046	25,101	2210
Jul.	0.86	39,606	36,528	2336
Aug.	0.83	37,832	24,852	2188
Sep.	0.77	34,238	21,608	1902
Oct.	0.86	29,413	19,701	1735
Nov.	0.85	24,909	16,577	1460
Dec.	0.80	22,669	14,599	1285

[a]Monthly averaged, daily extraterrestrial radiation.

The high levels of radiation predicted above are typical of the North Sahel region and are higher than most U.S. locations except the Mojave Desert.

A number of researchers found Angström-Page type correlations for specific locations which are listed in Table 2.6. Some of these include additional parameters such as

Table 2.5. Coefficients *a* and *b* in the Angström-Page regression equation[+]

Location	Climate[++]	Sunshine hours in percentage of possible Range	Avg.	*a*	*b*
Albuquerque, NM	BS-BW	68–85	78	0.41	0.37
Atlanta, GA	Cf	45–71	59	0.38	0.26
Blue Hill, MA	Df	42–60	52	0.22	0.50
Brownsville, TX	BS	47–80	62	0.35	0.31
Buenos Aires, Arg.	Cf	47–68	59	0.26	0.50
Charleston, SC	Cf	60–75	67	0.48	0.09
Dairen, Manchuria	Dw	55–81	67	0.36	0.23
El Paso, TX	BW	78–88	84	0.54	0.20
Ely, NV	BW	61–89	77	0.54	0.18
Hamburg, Germany	Cf	11–49	36	0.22	0.57
Honolulu, HI	Af	57–77	65	0.14	0.73
Madison, WI	Df	40–72	58	0.30	0.34
Malange, Angola	Aw-BS	41–84	58	0.34	0.34
Miami, FL	Aw	56–71	65	0.42	0.22
Nice, France	Cs	49–76	61	0.17	0.63
Poona, India (monsoon)	Am	25–49	37	0.30	0.51
(dry)		65–89	81	0.41	0.34
Stanleyville, Congo	Af	34–56	48	0.28	0.39
Tamanrasset, Algeria	BW	76–88	83	0.30	0.43

[+]From Löf et al. [46] with permission.

[++] Af = tropical forest climate, constantly moist, rainfall all through the year
Am = tropical forest climate, monsoon rain, short dry season, but total rainfall sufficient to support rain forest
Aw = tropical forest climate, dry season in winter
BS = steppe or semiarid climate
BW = desert or arid climate
Cf = mesothermal forest climate, constantly moist, rainfall all through the year
Cs = mesothermal forest climate, dry season in winter
Df = microthermal snow forest climate, constantly moist, rainfall all through the year
Dw = microthermal snow forest climate, dry season in winter

relative humidity and ambient temperature. Correlations listed in the table may be used for the specific locations for which they were developed.

Another meteorological variable that could be used for solar radiation prediction is the opaque cloud cover recorded at many weather stations around the world. This quantity is a measure of the percent of the sky dome obscured by opaque clouds. Because this parameter contains even less solar information than sunshine values, it has not been useful in predicting long-term solar radiation values. A subsequent section, however, will show that cloud cover, when used with solar altitude angle or air mass, is a useful estimator of hourly direct radiation.

Table 2.6. Angström-Page type correlations for specific locations

Authors	Measured data correlated	Correlation equations*
Iqbal [28]	Canada, 3 locations	$\frac{\bar{D}_h}{\bar{H}_h} = 0.791 - 0.635\left(\frac{\bar{n}}{\bar{N}}\right)$ $\frac{\bar{H}_d}{\bar{H}_h} = 0.163 + 0.478\left(\frac{\bar{n}}{\bar{N}}\right) - 0.655\left(\frac{\bar{n}}{\bar{N}}\right)^2$ $\frac{\bar{H}_b}{\bar{H}_{o,h}} = -0.176 + 1.45\left(\frac{\bar{n}}{\bar{N}}\right) - 1.12\left(\frac{\bar{n}}{\bar{N}}\right)^2$
Garg [17]	India, 11 locations, 20 years' data	$\frac{\bar{H}_h}{\bar{H}_{o,h}} = 0.3156 + 0.4520\left(\frac{\bar{n}}{\bar{N}}\right)^2$ $\frac{\bar{D}_h}{\bar{H}_{o,h}} = 0.3616 - 0.2123\left(\frac{\bar{n}}{\bar{N}}\right)$ $\frac{\bar{D}_h}{\bar{H}_h} = 0.8677 - 0.7365\left(\frac{\bar{n}}{\bar{N}}\right)$
Hussain [25]	India	$\frac{\bar{H}_h}{\bar{H}_{o,h}} = 0.394 + 0.364\left[\frac{\bar{n}}{\bar{N}'}\right] - 0.0035W_{at}$ $\frac{\bar{D}_h}{\bar{H}_{o,h}} = 0.306 - 0.165\left[\frac{\bar{n}}{\bar{N}'}\right] - 0.0025W_{at}$
Coppolino [11]	Italy	$\frac{\bar{H}_h}{\bar{H}_{o,h}} = 0.67\left(\frac{\bar{n}}{\bar{N}}\right)^{0.45} \sin(\alpha_{sn})^{0.05}$ α_{sn} = Solar Elevation at noon on the 15th of each month, degrees $0.15 \leq \frac{\bar{n}}{\bar{N}} \leq 0.90$
Akinoglu & Ecevit [2]	Italy	$\frac{\bar{H}_h}{\bar{H}_{o,h}} = 0.145 + 0.845\left(\frac{\bar{n}}{\bar{N}}\right) - 0.280\left(\frac{\bar{n}}{\bar{N}}\right)^2$
Ögelman et al. [56]	Turkey, 2 locations, 3 years' data	$\left(\frac{\bar{H}_h}{\bar{H}_{o,h}}\right) = 0.204 + 0.758\left(\frac{\bar{n}}{\bar{N}}\right) - 0.250\left\{\left[\left(\frac{\bar{n}}{\bar{N}}\right)^2\right]^2 + \sigma^2_{\frac{\bar{n}}{\bar{N}}}\right\}$ $\sigma^2_{\frac{\bar{n}}{\bar{N}}} = 0.035 + 0.326\left(\frac{\bar{n}}{\bar{N}}\right) - 0.433\left(\frac{\bar{n}}{\bar{N}}\right)^2$

Table 2.6. ***(Continued)***

Authors	Measured data correlated	Correlation equations*
Gopinathan [19]	40 locations around the world	$\frac{\overline{H}_h}{\overline{H}_{o,h}} = a + b\left(\frac{\overline{n}}{\overline{N}}\right)$ $a = -.309 + .539 \cos L - .0639\, h + 0.290\left(\frac{\overline{n}}{\overline{N}}\right)$ $b = 1.527 - 1.027 \cos L + .0926\, h - .359\left(\frac{\overline{n}}{\overline{N}}\right)$

*$\overline{H}_a$, $\overline{H}_b$, $\overline{H}_{o,h}$, $\overline{D}_h$ are monthly averaged daily values.
$\overline{N}'$ = maximum duration for which Campbell-Stokes recorder can be active, i.e., Solar Elevation >5°.
W_{at} = relative humidity × $(4.7923 + 0.3647T + 0.055T^2 + 0.0003T^3$
T = ambient temperature °C
W_{at} = gm moisture/m^3
h = Elevation in km above sea level.
L = latitude

2.6 MODELS BASED ON LONG-TERM MEASURED HORIZONTAL SOLAR RADIATION

Long-term measured solar radiation data is usually available as monthly averaged total solar radiation per day on horizontal surfaces. In order to use this data for tilted surfaces, the total solar radiation on a horizontal surface must first be broken down into beam and diffuse components. A number of researchers have proposed models to do that, prominent among them being Liu and Jordan, Collares-Pereira and Rabl, and Erbs, Duffie and Klein.

2.6.1 Monthly Solar Radiation on Tilted Surfaces

In a series of papers, Liu and Jordan [41–45] have developed an essential simplification in the basically complex computational method required to calculate long-term radiation on tilted surfaces. This is called the LJ method. The fundamental problem in such calculations is the decomposition of long-term measured total horizontal radiation into its beam and diffuse components.

If the decomposition can be computed, the trigonometric analysis presented earlier can be used to calculate incident radiation on any surface in a straightforward manner. Liu and Jordan (LJ) correlated the diffuse-to-total radiation ratio ($\overline{D}_h/\overline{H}_h$) with the ***monthly clearness index*** $\overline{K}_T$, which is defined as

$$\overline{K}_T = \frac{\overline{H}_h}{\overline{H}_{o,h}}, \tag{2.50}$$

where $\overline{H}_h$ is the monthly averaged terrestrial radiation per day on a horizontal surface. $\overline{H}_{o,h}$ is the corresponding extraterrestrial radiation, which can be calculated from Eq.

(2.49) by averaging each daily total for a month. The original LJ method was based upon the extraterrestrial radiation at midmonth, which is not truly an average.

The LJ correlation predicts the monthly diffuse ($\overline{D}_h$) to monthly total $\overline{H}_h$ ratio. It can be expressed by the empirical Eq.

$$\frac{\overline{D}_h}{\overline{H}_h} = 1.390 - 4.027\,\overline{K}_T + 5.531\overline{K}_T^2 - 3.108\overline{K}_T^3 . \tag{2.51}$$

Note that the LJ correlation is based upon a solar constant value of 1394 W/m^2 (442 Btu/hr · ft^2), which was obtained from terrestrial observations, whereas the newer value, based on satellite data, is 1377 W/m^2 (437 Btu/hr · ft^2). The values of $\overline{K}_T$ must be based on this earlier value of the solar constant to use the LJ method. Collares-Pereira and Rabl [10] conducted a study and concluded that although Liu and Jordan's approach is valid, their correlations would predict significantly smaller diffuse radiation components. They also concluded that Liu and Jordan were able to correlate their model with the measured data because they used the measured data which was not corrected for the shade ring (see solar radiation measurements). Collares-Pereira and Rabl (C-P&R) also introduced the sunset hour angle h_{ss} in their correlation to account for the seasonal variation in the diffuse component. The C-P&R correlation is:

$$\frac{\overline{D}_h}{\overline{H}_h} = 0.775 + 0.347\left(h_{ss} - \frac{\pi}{2}\right) - \left[0.505 + 0.0261\left(h_{ss} - \frac{\pi}{2}\right)\right]\cos(2K_T - 1.8), \tag{2.52}$$

where h_{ss} is the sunset hour angle in radians. The C-P&R correlation agrees well with the correlations for India [8], Israel [71] and Canada [66] and is, therefore, preferred to equation (2.51).

The monthly average beam component $\overline{B}_h$ on a horizontal surface can be readily calculated by simple subtraction since $\overline{D}_h$ is known:

$$\overline{B}_h = \overline{H}_h - \overline{D}_h. \tag{2.53}$$

It will be recalled on an instantaneous basis from Eqs. (2.41) and (2.43) and Fig. (2.19) that

$$I_{b,N} = \frac{I_{b,h}}{\sin\alpha}, \tag{2.54}$$

$$I_{b,c} = I_{b,N}\cos i, \tag{2.43}$$

where $I_{b,h}$ is the instantaneous horizontal beam radiation. Solving for $I_{b,c}$, the beam radiation on a surface,

$$I_{b,c} = I_{b,h}\left(\frac{\cos i}{\sin\alpha}\right). \tag{2.55}$$

The ratio in parentheses is usually called the beam radiation ***tilt factor*** R_b. It is a purely geometric quantity that converts instantaneous horizontal beam radiation to beam radiation intercepted by a tilted surface.

Equation (2.55) cannot be used directly for the long-term beam radiation $\overline{B}_h$. To be strictly correct, the instantaneous tilt factor R_b should be integrated over a month with the beam component $I_{b,h}$ used as a weighting factor to calculate the beam tilt factor. However, the LJ method is used precisely when such short-term data as $I_{b,h}$ are not available. The LJ recommendation for the monthly mean tilt factor $\overline{R}_b$ is simply to calculate the monthly average of cos i and divide it by the same average of sin α. In equation form for south-facing surfaces, this operation yields:

$$\overline{R}_b = \frac{\cos(L - \beta)\cos\delta_s \sin h_{sr} + h_{sr} \sin(L - \beta) \sin\delta_s}{\cos L \cos\delta_s \sin h_{sr}\,(\alpha = 0) + h_{sr}(\alpha = 0) \sin L \sin \delta_s}, \tag{2.56}$$

where the sunrise hour angle $h_{sr}(\alpha = 0)$ in radians is given by Eq (2.30) and h_{sr} is the min $[|h_s\ (\alpha = 0)|, |h_s\ (i = 90°)|]$, respectively, and are evaluated at midmonth. Non-south-facing surfaces require numerical integration or iterative methods to determine $\overline{R}_b$. The long-term beam radiation on a tilted surface $\overline{B}_c$ is then,

$$\overline{B}_c = \overline{R}_b\, \overline{B}_h, \tag{2.57}$$

which is the long-term analog of Eq. (2.43). Values of $\overline{R}_b$ are tabulated in Appendix 2, Table A2.5.

Diffuse radiation intercepted by a tilted surface differs from that on a horizontal surface, because a tilted surface does not view the entire sky dome, which is the source of diffuse radiation. If the sky is assumed to be an isotropic source of diffuse radiation, the instantaneous and long-term tilt factors for diffuse radiation, R_d and $\overline{R}_d$ respectively, are equal and are simply the radiation view factor from the plane to the visible portion of a hemisphere. In equation form:

$$R_d = \overline{R}_d = \cos^2\frac{\beta}{2} = (1 + \cos\beta)/2. \tag{2.58}$$

In some cases where solar collectors are mounted near the ground, some beam and diffuse radiation reflected from the ground can be intercepted by the collector surface. The tilt factor $\overline{R}_r$ for reflected total radiation $(\overline{D}_h + \overline{B}_h)$ is then calculated to be

$$\overline{R}_r = \frac{\overline{R}}{\overline{D}_h + \overline{B}_h} = \rho \sin^2\frac{\beta}{2} = \rho(1 - \cos\beta)/2, \tag{2.59}$$

in which ρ is the diffuse reflectance of the surface south of the collector assumed uniform and of infinite extent.

For snow, $\rho \cong 0.75$; for grass and concrete, $\rho \cong 0.2$. A more complete list of reflectances is provided in Table A2.7 of Appendix 2. The total long-term radiation inter-

cepted by a surface $\overline{H}_c$ is then the total of beam, diffuse, and diffusely reflected components:

$$\overline{H}_c = \overline{R}_b \overline{B}_h + \overline{R}_d \overline{D}_h + \overline{R}_r(\overline{D}_h + \overline{B}_h). \tag{2.60}$$

Using Eqs. (2.61) and (2.62), we have

$$\overline{H}_c = \overline{R}_b\overline{B}_h + \overline{D}_h \cos^2\frac{\beta}{2} + (\overline{D}_h + \overline{B}_h)\rho \sin^2\frac{\beta}{2}, \tag{2.61}$$

in which $\overline{R}_b$ is calculated from Eq. (2.56).

Example 2.8. Using the $\overline{H}_h$ data calculated in Example 2.7 in place of the long-term measured data for the North Central Sahara Desert at latitude 25°N, find the monthly averaged insolation per day on a south-facing solar collector tilted at an angle of 25° from the horizontal.

Solution. The solution below is for the month of January. Values for the other months can be found by following the same method.

$$\overline{H}_h = 16{,}215\text{kJ/m}^2 - \text{day}.$$

From Table A2.2a:

$$\overline{H}_{o,h} = 23{,}902.$$

Therefore,

$$\overline{K}_T = \overline{H}_h/\overline{H}_{o,h} = 0.678.$$

δ_s and h_{sr} can be found for the middle of the month (January 16).

$$\begin{aligned}\delta_s &= 23.45° \sin[360(284 + 16)365]° \\ &= -21.1°, \\ h_{sr}(\alpha = 0) &= -\cos^{-1}(-\tan L \tan \delta) \\ &= -79.6° \text{ or } -1.389\text{rad}. \\ \text{and } h_{ss} &= 1.389\end{aligned}$$

Using CP & R correlation,

$$\frac{\overline{D}_h}{H_h} = 0.775 + 0.347(1.389 - 1.5708)$$
$$- [0.505 + 0.0261(1.389 - 1.5708)]\cos(2 \times 0.678 - 1.8)$$
$$= 0.212$$

Therefore,

$$\overline{D}_h = 0.212 \times 16{,}215 = 3{,}438\text{kJ/m}^2 - \text{day}$$
$$\text{and } \overline{B}_h = \overline{H}_h - \overline{D}_h = 12{,}777\text{kJ/m}^2 - \text{day}$$

Insolation on a tilted surface can be found from Eq. (2.60). We need to find $\overline{R}_B$ from Eq. (2.56).

Therefore,

$$\overline{R}_b = \frac{\cos(0)\cos(-21.1°)\sin(-79.6°) - 1.389\sin(0)\sin(-21.1°)}{\cos(25°)\cos(-21.1°)\sin(-79.6°) - 1.389\sin(25°)\sin(-21.1°)}$$
$$= 147.$$

$$\overline{R}_d = \cos^2(25/2) = 0.953.$$
$$\overline{R}_r = \rho \sin^2(\beta/2) \text{ (Assume } \rho = 0.2)$$
$$= 0.2 \sin^2(12.5°)$$
$$= 0.009.$$

Therefore,

$$\overline{H}_c = (1.47)(12{,}777) + 0.953(3{,}438) + 0.009(16{,}215)$$
$$= 22{,}205 \text{ kJ/m}^2.$$

2.6.2 Circumsolar or Anisotropic Diffuse Solar Radiation

The models described in the above sections assume that the sky diffuse radiation is isotropic. However, this assumption is not true because of circumsolar radiation (brightening around the solar disk). Although the assumption of isotropic diffuse solar radiation does not introduce errors in the diffuse values on horizontal surfaces, it can result in errors of 10 to 40% in the diffuse values on tilted surfaces. A number of researchers have studied the anisotropy of the diffuse solar radiation because of circumsolar radiation. Temps and Coulson [73] introduced an anisotropic diffuse radiation algorithm for tilted surfaces for clear sky conditions. Klucher [37] refined the Temps and Coulson algorithm by adding a cloudiness function to it:

$$R_d = \frac{1}{2}(1 + \cos\beta)M_1M_2, \tag{2.62}$$

where

$$M_1 = 1 + F\sin^3(\beta/2), \tag{2.63}$$

$$M_2 = 1 + F\cos^2 i \sin^3(z), \text{ and} \tag{2.64}$$

$$F = 1 - (D_h/H_h)^2. \tag{2.65}$$

Examining F, we find that under overcast skies ($D_h = H_h$), R_d in Eq. 2.62 reduces to the isotropic term of Liu and Jordan. The Klutcher algorithm reduces the error in diffuse radiation to about 5%.

In summary, monthly averaged, daily solar radiation on a surface is calculated by first decomposing total horizontal radiation into its beam and diffuse components using Eq. (2.51) or (2.52). Various tilt factors are then used to convert these horizontal components to components on the surface of interest.

2.6.3 Daily Solar Radiation on Tilted Surfaces

Prediction of daily horizontal total solar radiation for sites where solar data are not measured can be done using the Angström-Page model. Instead of monthly values, however, daily values are used for percent sunshine *PS* and extraterrestrial radiation I_{day}. The results of using this simple model would be expected to show more scatter than monthly values, however.

All U.S. National Weather Service (NWS) stations with solar capability report daily horizontal total (beam and diffuse) radiaton. Liu and Jordan have extended their monthly method described above to apply to daily data. The equation, analogous to Eq. (2.51), used to calculate the daily diffuse component $\bar{I}_{d,h}$ is [6]

$$\frac{\bar{I}_{d,h}}{\bar{I}_h} = 1.0045 + 0.04349K_T - 3.5227K_T^2 + 2.6313K_T^3, \text{ and} \tag{2.66}$$

$$K_T \leq 0.75,$$

where K_T (no overbar) is the daily clearness index analogous to the monthly $\bar{K}_T$. (In this section, overbars indicate daily radiation totals.) For values of $K_T > 0.75$, the diffuse-to-total ratio is constant at a value of 0.166. K_T is given by

$$K_T = \frac{\bar{I}_h}{\bar{I}_{o,h}}. \tag{2.67}$$

The daily extraterrestrial total radiation $\bar{I}_{o,h}$ is calculated from Eq. (2.49). Note that Eq. (2.66) is based on the early solar constant value of 1394 W/m^2 (442 Btu/hr · ft^2).

The daily horizontal beam component $\bar{I}_{b,h}$ is given by simple subtraction:

$$\bar{I}_{b,h} = \bar{I}_h - \bar{I}_{d,h}. \tag{2.68}$$

The beam, diffuse, and reflected components of radiation can each be multiplied by their tilt factors R_b, R_d, and R_r to calculate the total radiation on a tilted surface

$$\bar{I}_c = R_b\bar{I}_{b,h} + R_d\bar{I}_{d,h} + R_r(\bar{I}_{b,h} + \bar{I}_{d,h}), \tag{2.69}$$

in which

$$R_b = \frac{\cos(L - \beta)\cos\delta_s \sin h_{sr} + h_{sr}\sin(L - \beta)\sin\delta_s}{\cos L \cos\delta_s \sin h_{sr}(\alpha = 0) + h_{sr}(\alpha = 0)\sin L \sin\delta_s}, \tag{2.70}$$

$$R_d = \cos^2\frac{\beta}{2}, \text{ and} \tag{2.71}$$

$$R_r = \rho \sin^2\frac{\beta}{2}, \tag{2.72}$$

by analogy with the previous, monthly analysis.

If daily solar data are available, they can be used for design, the same as monthly data. Daily calculations are necessary when finer time-scale performance is required. In addition, daily data can be decomposed into hourly data, which are useful for calculations made with large, computerized solar system simulation models.

2.6.4 Hourly Solar Radiation on Tilted Surfaces

Hourly solar radiation can be predicted in several ways. Correlations between hourly total and hourly diffuse (or beam) radiation or meteorological parameters such as cloud cover or air mass may be used. Alternatively, a method proposed by Liu and Jordan based on the disaggregation of daily data into hourly data could be used [41–45]. Even if hourly NWS data are available, it is necessary to decompose these total values into beam and diffuse components depending upon the response of the solar conversion device to be used to these two fundamentally different radiation types.

Randall and Leonard [62] have correlated historical data from the NWS stations at Blue Hill, Massachusetts, and Albuquerque, New Mexico to predict ***hourly beam radiation*** I_b and ***hourly total horizontal radiation*** I_h. This method can be used to decompose NWS data into its beam and diffuse components.

The hourly beam radiation was found to be fairly well correlated by hourly ***percent of possible insolation*** k_t, defined as

$$k_t = \frac{I_h}{I_{o,h}}, \tag{2.73}$$

in which $I_{o,h}$ is the hourly horizontal extraterrestrial radiation, which can be evaluated from Eq. (2.49) using one-hour integration periods. Carrying out the integration over a one hour period yields

$$I_{o,h} = I_o\left(1 + 0.034 \cos\frac{360n}{365}\right)(0.9972 \cos L \cos\delta_s \cos h_s + \sin L \sin \delta_s), \quad (2.74)$$

where the solar hour angle h_s is evaluated at the center of the hour of interest.

The direct normal-beam correlation based on k_t is [45]

$$I_{b,N} = -520 + 1800k_t (W/m^2) \quad 0.85 > k_t \geq 0.30 \quad (2.75)$$

$$I_{b,N} = 0 \quad k_t < 0.30 \quad (2.76)$$

This fairly simple correlation gives more accurate $I_{b,N}$ values than the more cumbersome Liu and Jordan procedure, at least for Blue Hill and Albuquerque. Vant-Hull and Easton [80] have also devised an accurate predictive method for beam radiation.

Randall and Leonard [62] have made a correlation of *total* horizontal hourly radiation $I_h(W/m^2)$ on the basis of *opaque cloud cover CC* and *air mass m* using data for Riverside, Los Angeles, and Santa Monica, California. Cloud cover is defined as $CC = 1.0$ for fully overcast and $CC = 0.0$ for clear skies. A polynomial fit was used:

$$I_h = \frac{I_{o,h}}{100}(83.02 - 3.847m - 4.407CC + 1.1013CC^2 - 0.1109CC^3) \quad (2.77)$$

The average predictive error for this correlation was ± 2.3 percent of the NWS data; the correlation coefficient of I_h with CC is 0.76 for the data used. Equation (2.80) was used to predict I_h for Inyokern, California, a site not used in the original correlation. Predictions of solar radiation for Inyokern were within 3.2 percent of NWS. The diffuse radiation can be calculated from Eqs. (2.75), (2.76), and (2.77):

$$I_{d,h} = I_h - I_b \sin\alpha \quad (2.78)$$

The American Society of Heating, Refrigerating, and Air Conditioning Engineers (ASHRAE) has calculated hourly clear-sky values on vertical, horizontal, and tilted surfaces. One table for a full year has been prepared for each of six values of latitude spanning the continental United States. In addition, tables of solar azimuth and altitude angle have been prepared for the same six latitudes. The solar radiation data represent the maximum that could be expected on a clear day and are therefore of limited usefulness in the design of solar systems. They can be used, however, to calculate cooling loads on buildings and the like. The ASHRAE tables are contained in Appendix 2.

supersaturated fluosilicic acid solution, the acid attacks the glass and leaves a porous silica surface layer. This layer has an index of refraction intermediate between glass and air. Figure 3.5 shows the spectral reflectance of a pane of glass before and after etching.

3.2 FLAT PLATE COLLECTORS

A simple flat plate collector consists of an absorber surface (usually a dark, thermally conducting surface); a trap for reradiation losses from the absorber surface (such as glass which transmits shorter wavelength solar radiation but blocks the longer wavelength radiation from the absorber); a heat transfer medium such as air, water, etc.; and some thermal insulation behind the absorber surface. Flat plate collectors are used typically for temperature requirements up to 75°C although higher temperatures can be obtained from high efficiency collectors. These collectors are of two basic types based on the heat transfer fluid:

Liquid type: where heat transfer fluid may be water, mixture of water and antifreeze, oil, etc.;
Air type: where heat transfer medium is air (used mainly for drying and space heating requirements).

3.2.1 Liquid-Type Collectors

Figure 3.6 shows a typical liquid-type flat plate collector. In general it consists of:

1. *Glazing*: one or more covers of transparent material like glass, plastics, etc. Glazing may be left out for some low-temperature applications.

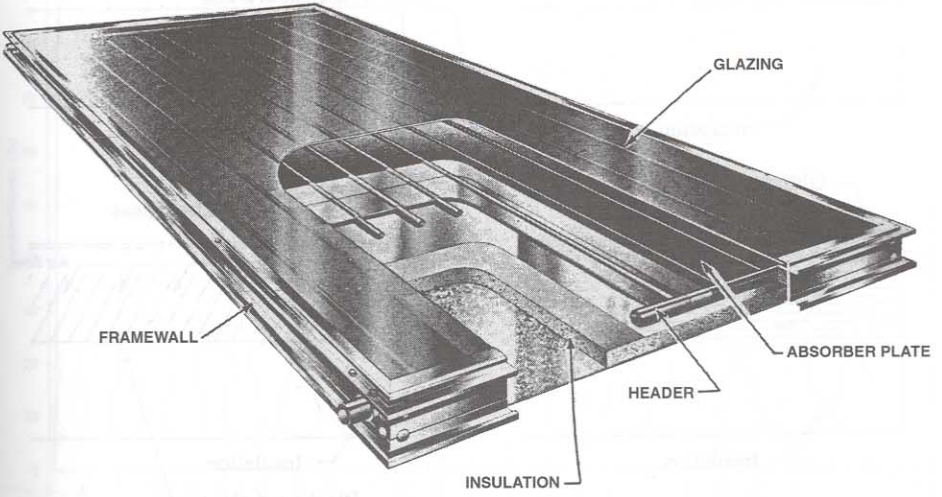

Figure 3.6. Typical liquid-type flat plate collector (courtesy of Morning Star Corporation, Orange Park, Florida).

2. ***Absorber***: a plate with tubes or passages attached to it for the passage of a working fluid. The absorber plate is usually painted flat black or electroplated with a selective absorber.
3. ***Headers*** or manifolds: to facilitate the flow of heat transfer fluid.
4. ***Insulation***: to minimize heat loss from the back and the sides.
5. ***Container***: box or casing.

3.2.2 Air-Type Collectors

Air types of collectors are more commonly used for agricultural drying and space heating applications. Their basic advantages are low sensitivity to leakage and no need for an additional heat exchanger for drying and space heating applications. However, because of the low heat capacity of the air and the low convection heat transfer coefficient between the absorber and the air, a larger heat transfer area and higher flow rates are needed. Figure 3.7 shows some common configurations of air heating collectors. Common absorber materials include corrugated aluminum or galvanized steel sheets, black metallic screens, or simply any black painted surface.

Unglazed, transpired solar air collectors offer a low-cost opportunity for some applications such as preheating of ventilation air and agricultural drying and curing [49]. Such collectors consist of perforated absorber sheets that are exposed to the sun and through which air is drawn. The perforated absorber sheets are attached to the vertical walls, which are exposed to the sun. Kutcher and Christensen [50] have given a de-

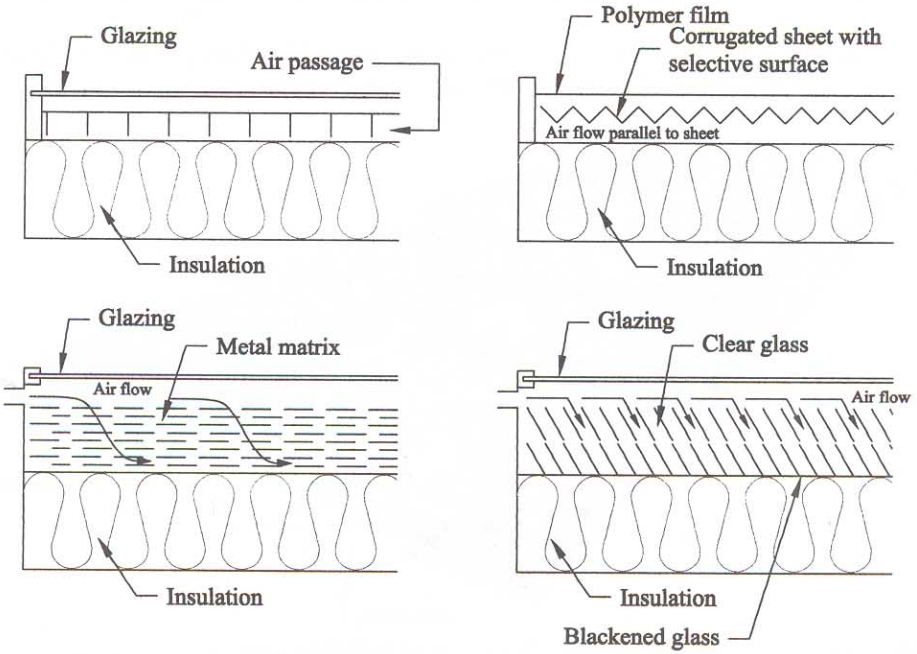

Figure 3.7. Some common configurations of air heating collectors.

tailed thermal analysis of unglazed transpired solar collectors. (See Chapter 5, Section 5.4.5 for additional details.)

The most important components, whose properties determine the efficiency of solar thermal collectors, are glazings and absorbers.

3.2.3 Glazings

The purpose of a glazing or transparent cover is to transmit the shorter wavelength solar radiation but block the longer wavelength reradiation from the absorber plate, and to reduce the heat loss by convection from the top of the absorber plate. Consequently, an understanding of the process and laws that govern the transmission of radiation through a transparent medium is important. Section 3.1 describes in brief the transmission of radiation through materials.

Glass is the most common glazing material. Figure 3.8 shows transmittance of glass as a function of wavelength. Transparent plastics, such as polycarbonates and acrylics are also used as glazings for flat plate collectors. The main disadvantage of plastics is that their transmittance in the longer wavelength is also high, therefore, they are not as good a trap as glass. Other disadvantages include deterioration over a period of time due to ultraviolet solar radiation. Their main advantage is resistance to breakage. Although glass can break easily, this disadvantage can be minimized by using tempered glass.

In order to minimize the upward heat loss from the collector, more than one transparent glazing may be used. However, with the increase in the number of cover plates, transmittance is decreased. Figure 3.9 shows the effect of number of glass cover plates on transmittance.

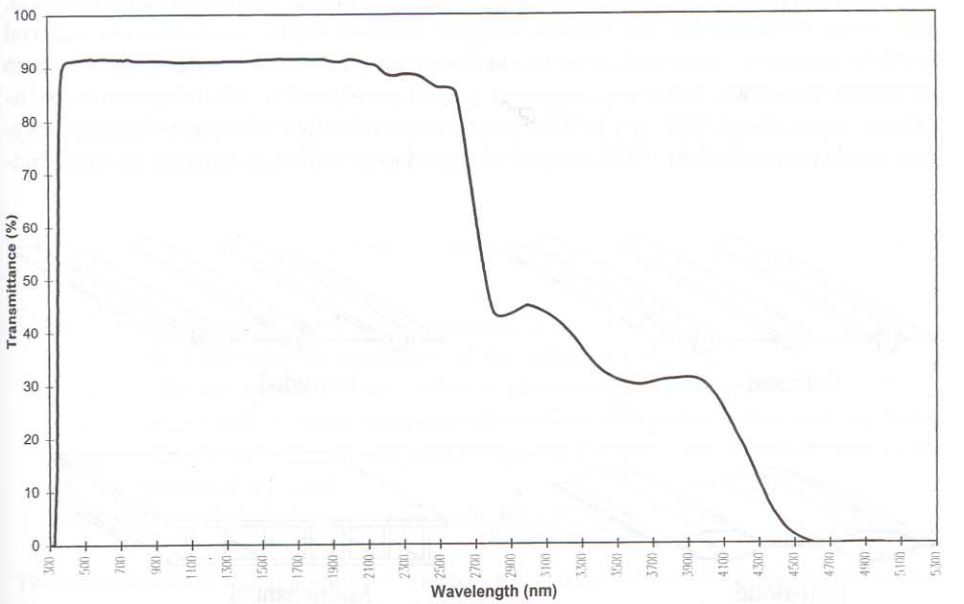

Figure 3.8. Spectral transmittance of 3 mm Low Iron Float glass.

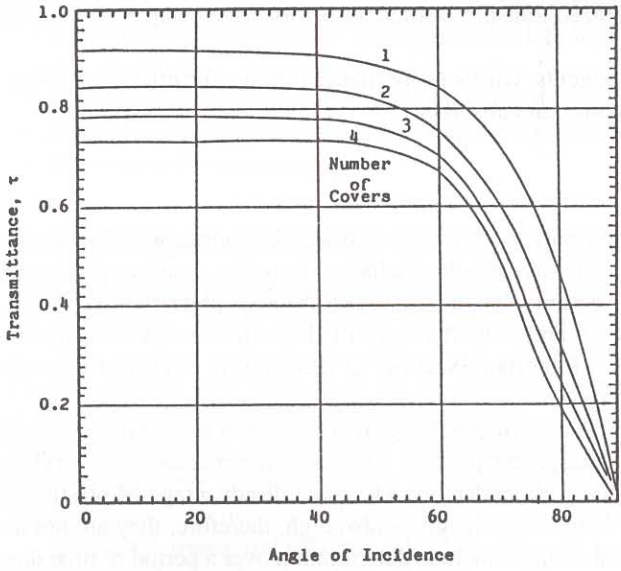

Figure 3.9. Transmittance of multiple glass covers having an index of refraction 1.526″.

Absorbers. The purpose of the absorber is to absorb as much of the incident solar radiation as possible, re-emit as little as possible, and allow efficient transfer of heat to a working fluid. The most common forms of absorber plates in use are shown in Figure 3.10. The materials used for absorber plates include copper, aluminum, stainless steel, galvanized steel, plastics and rubbers. Copper seems to be the most common material used for absorber plates and tubes because of its high thermal conductivity and high corrosion resistance. However, copper is quite expensive. For low-temperature applications (up to about 50°C or 120°F) a plastic material called ethylene propylene polymer (trade names EPDM, HCP, etc.) can be used to provide inexpensive absorber ma-

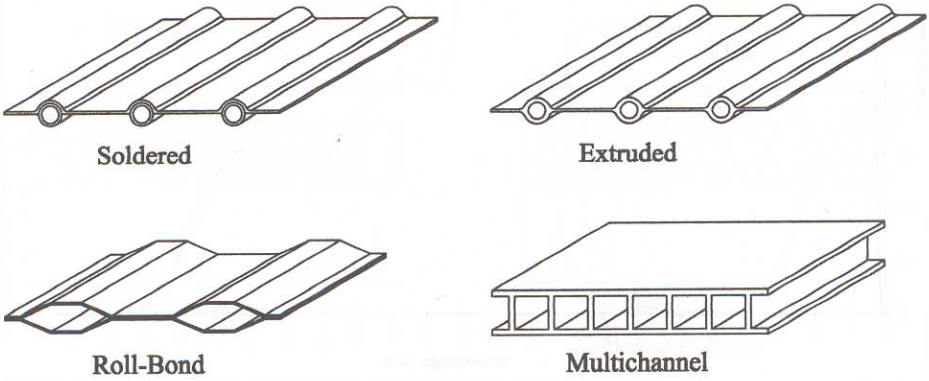

Figure 3.10. Common types of absorber plates.

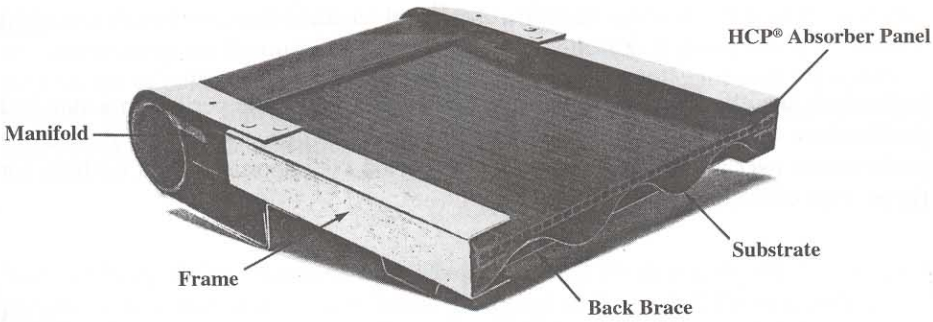

Figure 3.11. Cutaway view of a typical collector made from ethylene propylene polymer (Courtesy of Sealed Air Corporation, Saddlebrook, NJ).

terial. To compensate for the low thermal conductivity, a large surface area is provided for heat transfer. Figure 3.11 shows a typical collector made from such material.

In order to increase the absorption of solar radiation and to reduce the emission from the absorber, the metallic absorber surfaces are painted or coated with flat black paint or some selective coating. A selective coating has high absorptivity in the solar wavelength range (0.3 to 3.0 μm). Absorptivities and emissivities of some common selective surfaces are given in Table 3.3.

A simple and inexpensive collector consists of a black painted corrugated metal absorber on which water flows down open, rather than enclosed in tubes. This type of collector is called a ***trickle collector*** and is usually built on-site. Although such a collector is simple and inexpensive, it has the disadvantages of condensation on the glazing and a higher pumping power requirement.

3.2.4 Energy balance for a flat-plate collector. The thermal performance of any type of solar thermal collector can be evaluated by an energy balance that determines the portion of the incoming radiation delivered as useful energy to the working fluid. For a flat-plate collector of an area A_c this energy balance on the absorber plate is

$$I_c A_c \tau_s \alpha_s = q_u + q_{loss} + \frac{de_c}{dt}, \tag{3.8}$$

where I_c = solar irradiation on a collector surface,
τ_s = effective solar transmittance of the collector cover(s),
α_s = solar absorptance of the collector-absorber plate surface,
q_u = rate of heat transfer from the collector-absorber plate to the working fluid,
q_{loss} = rate of heat transfer (or heat loss) from the collector-absorber plate to the surroundings, and
de_c/dt = rate of internal energy storage in the collector.

The instantaneous efficiency of a collector η_c is simply the ratio of the useful energy delivered to the total incoming solar energy, or

$$\eta_c = \frac{q_u}{A_c I_c}. \tag{3.9}$$

In practice, the efficiency must be measured over a finite time period. In a standard performance test, this period is on the order of 15 or 20 min, whereas for design, the performance over a day or over some longer period t is important. Then we have for the average efficiency

$$\eta_c = \frac{\int_0^t q_u dt}{\int_0^t A_c I_c dt}, \tag{3.10}$$

where t is the time period over which the performance is averaged.

A detailed and precise analysis of the efficiency of a solar collector is complicated by the nonlinear behavior of radiation heat transfer. However, a simple linearized analysis is usually sufficiently accurate in practice. In addition, the simplified analytical procedure is very important because it illustrates the parameters of significance for a solar collector and how these parameters interact. For a proper analysis and interpretation of these test results an understanding of the thermal analysis is imperative, although for design and economic evaluation the results of standardized performance tests are generally used.

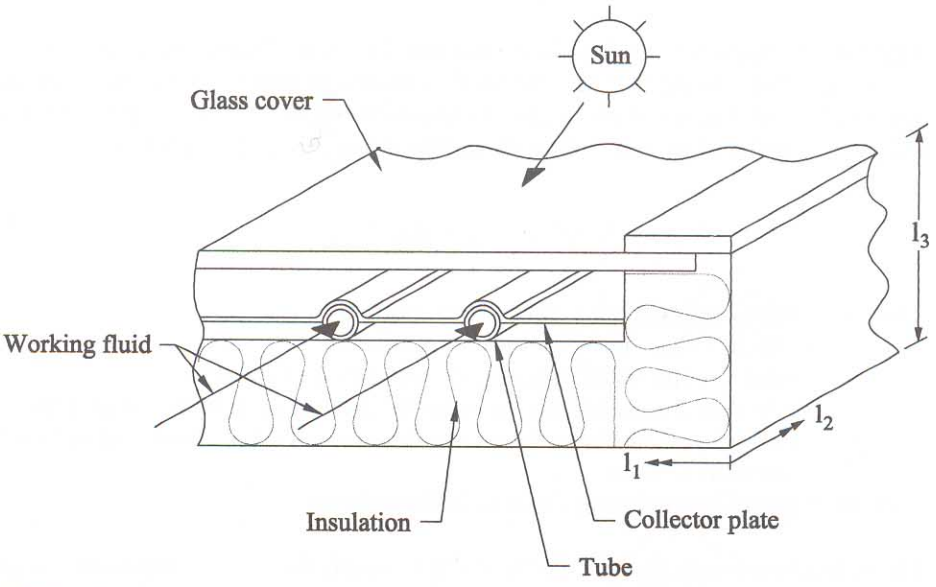

Figure 3.12. Schematic diagram of solar collector.

Collector heat-loss conductance. In order to obtain an understanding of the parameters determining the thermal-efficiency of a solar collector, it is important to develop the concept of ***collector heat-loss conductance***. Once the collector heat-loss conductance U_c is known, and when the collector plate is at an average temperature T_c, the collector heat loss can be written in the simple form

$$q_{loss} = U_c A_c (T_c - T_a) \tag{3.11}$$

The simplicity of this relation is somewhat misleading because the collector heat-loss conductance cannot be specified without a detailed analysis of all the heat losses. Figure 3.12 shows a schematic diagram of a single-glazed collector, while Fig. 3.13(a) shows the thermal circuit with all the elements that must be analyzed before they can be combined into a single conductance element shown in Figure 3.13(b). The analysis below shows an example of how this combination is accomplished.

In order to construct a model suitable for a thermal analysis of a flat-plate collector, the following simplifying assumptions will be made:

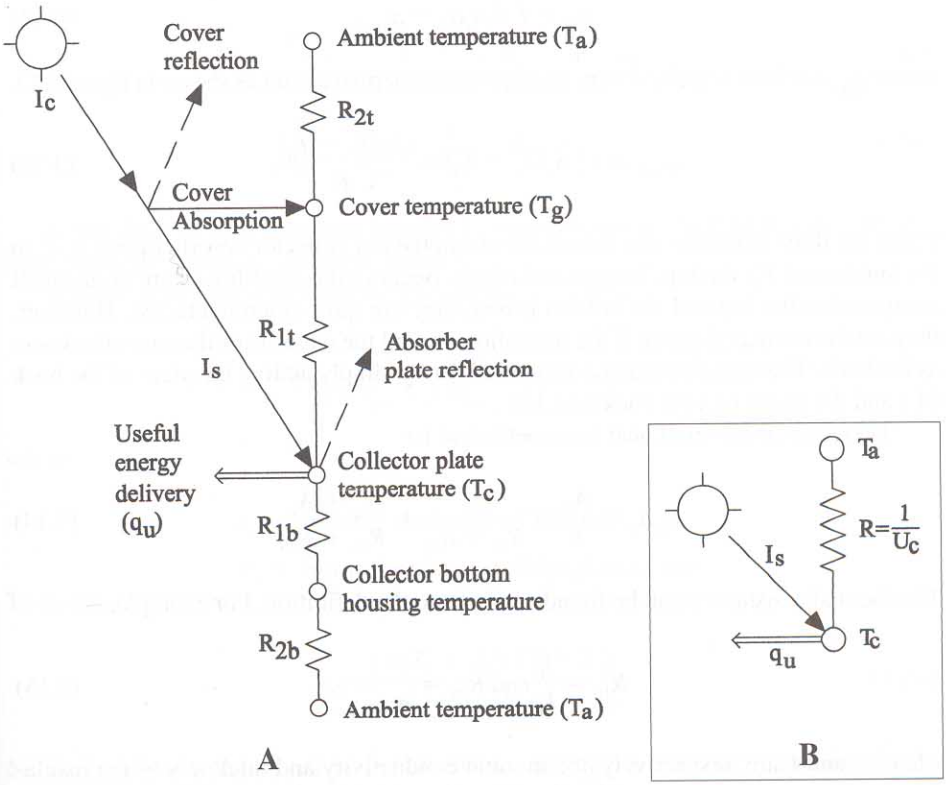

Figure 3.13. Thermal circuits for a flat-plate collector shown in Fig. 3.12: (a) detailed circuit; (b) approximate, equivalent circuit to (a). In both circuits, the absorber energy is equal to $\alpha_s I_s$, where $I_s = \tau_s I_c$. Collector assumed to be at uniform temperature T_c.

1. The collector is thermally in steady state.
2. The temperature drop between the top and bottom of the absorber plate is negligible.
3. Heat flow is one-dimensional through the cover as well as through the back insulation.
4. The headers connecting the tubes cover only a small area of the collector and provide uniform flow to the tubes.
5. The sky can be treated as though it were a black-body source for infrared radiation at an equivalent sky temperature.
6. The irradiation on the collector plate is uniform.

For a quantitative analysis let the plate temperature be T_c and assume solar energy is absorbed at the rate $I_s\alpha_s$. Part of this energy is then transferred as heat to the working fluid, and if the collector is in the steady state, the other part is lost as heat to the ambient air if $T_c > T_a$. Some of the heat loss occurs through the bottom of the collector. It passes first through the back to the environment. Since the collector is in steady state, according to Eq. (3.8),

$$q_u = I_c A_c \tau_s \alpha_s - q_{loss}, \tag{3.12}$$

where q_{loss} can be determined using the equivalent thermal circuit as shown in figure 3.13.

$$q_{loss} = U_c A_c (T_c - T_a) = \frac{A_c (T_c - T_a)}{R}. \tag{3.13}$$

There are three parallel paths to heat loss from the hot collector absorber plate at T_c to the ambient at T_a: the top, bottom and edges. Because the edge losses are quite small compared to the top and the bottom losses, they are quite often neglected. However, they can be estimated easily if the insulation around the edges is of the same thickness as the back. The edge loss can be accounted for by simply adding the areas of the back (A_c) and the edges (A_e) for back heat loss.

Therefore, the overall heat loss coefficient is:

$$U_c A_c = \frac{A_c}{R} = \frac{A_c}{R_{1t} + R_{2t}} + \frac{A_c + A_e}{R_{1b} + R_{2b}}. \tag{3.14}$$

The thermal resistances can be found easily from the definition. For example,

$$R_{1b} = \frac{l_i}{k_i} \text{ and } R_{2b} = \frac{1}{h_{c,bottom}}, \tag{3.15}$$

where k_i and l_i are, respectively, the thermal conductivity and thickness of the insulation, and $h_{c,bottom}$ is the convective heat transfer coefficient between the collector and the air below the collector. In a well-insulated collector, R_{2b} is much smaller than R_{1b} and usually neglected. Referring to figure 3.12

$$A_e = 2(l_1 + l_2)\, l_3 \tag{3.16}$$

Since the heat loss from the top is by convection and radiation, it is more complicated than the bottom heat loss. Convection and radiation provide two parallel paths for heat loss from the absorber plate at T_c to the glass cover at T_g, and from the glass cover to the ambient. That is, the series resistance of R_{1t} and R_{2t} consists of:

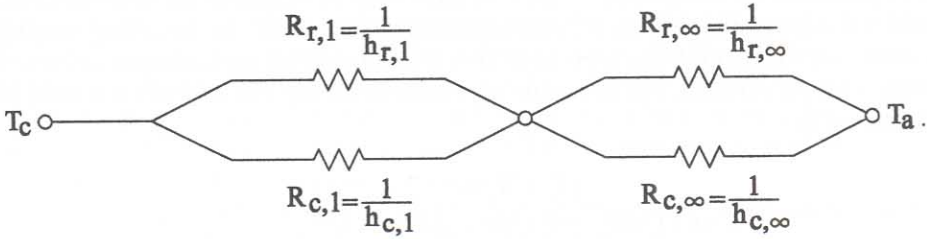

Therefore,

$$\frac{1}{R_{1t}} = \frac{1}{R_{r,1}} + \frac{1}{R_{c,1}} = h_{r,1} + h_{c,1} \text{ and} \tag{3.17}$$

$$\frac{1}{R_{2t}} = \frac{1}{R_{r,\infty}} + \frac{1}{R_{c,\infty}} = h_{r,\infty} + h_{c,\infty} \tag{3.18}$$

Since thermal radiative heat transfer is proportional to the fourth power of the temperature, R_r and h_r are found as follows:

Radiative heat transfer from the plate to the glass cover

$$q_{r_{c\to g}} = \sigma A_c \frac{(T_c^4 - T_g^4)}{(1/\epsilon_{p,i} + 1/\epsilon_{g,i} - 1)} = h_{r,1} A_c (T_c - T_g), \tag{3.19}$$

where

$\epsilon_{p,i}$ = infrared emittance of the plate

$\epsilon_{g,i}$ = infrared emittance of the glass cover.

Therefore,

$$h_{r,1} = \frac{\sigma(T_c + T_g)(T_c^2 + T_g^2)}{(1/\epsilon_{p,i} + 1/\epsilon_{g,i} - 1)}. \tag{3.20}$$

Similarly, from the radiative heat transfer between the glass plate (at T_g) and the sky (at T_{sky}) we can find that:

$$q_{r_{g\to sky}} = \epsilon_{g,i}\sigma A_c (T_g^4 - T_{sky}^4) = h_{r,\infty} A_c (T_g - T_a), \tag{3.21}$$

or

$$h_{r,\infty} = \epsilon_{g,i}\sigma(T_g^4 - T_{sky}^4)/(T_g - T_a). \tag{3.22}$$

Evaluation of the collector heat-loss conductance defined by Eq. (3.14) requires iterative solution of Eqs. (3.19) and (3.21), because the unit radiation conductances are functions of the cover and plate temperatures, which are not known a priori. A simplified procedure for calculating U_c for collectors with all covers of the same material, which is often sufficiently accurate and more convenient to use, has been suggested by Hottel and Woertz [36] and Klein [41]. It is also suitable for application to collectors with selective surfaces. For this approach the collector top loss in watts is written in the form [1]:

$$q_{toploss} = \frac{(T_c - T_a)A_c}{N/(C/T_c)[(T_c - T_a)/(N+f)]^{0.33} + 1/h_{c,\infty}} + \frac{\sigma(T_c^4 - T_a^4)A_c}{1/[\epsilon_{p,i} + 0.05N(1 - \epsilon_{p,i})] + (2N + f - 1)/\epsilon_{g,i} - N}, \tag{3.23}$$

where $f = (1 - 0.04h_{c,\infty} + 0.005h_{c,\infty}^2)(1 + 0.091N)$,
$C = 250[1 - 0.0044(\beta - 90)]$,
N = number of covers,
$h_{c,\infty} = 5.7 + 3.8V$, and
$\epsilon_{g,i}$ = infrared emittance of the covers,
V = wind speed in m/sec.

The values of $q_{top\ loss}$ calculated from Eq. (3.23) agreed closely with the values obtained from Eq. (3.22) for 972 different observations encompassing the following conditions:

$320 < T_c < 420$ K
$260 < T_a < 310$ K
$0.1 < \epsilon_{p,i} < 0.95$
$0 \leq V \leq 10$ m/sec
$1 \leq N \leq 3$
$0 \leq \beta \leq 90$

The standard deviation of the differences in $U_c = q_{top\ loss}/A_c(T_c - T_a)$ was 0.14 W/m^2 · K for these comparisons.

3.2.5 Thermal Analysis of Flat-Plate Collector-Absorber Plate

In order to determine the efficiency of a solar collector, the rate of heat transfer to the working fluid must be calculated. If transient effects are neglected [35,41,79], the rate of heat transfer to the fluid flowing through a collector depends on the temperature of

the collector surface from which heat is transferred by convection to the fluid, the temperature of the fluid, and the heat-transfer coefficient between the collector and the fluid. To analyze the rate of heat transfer consider first the condition at a cross section of the collector with flow ducts of rectangular cross sections as shown in Fig. 3.14. Solar radiant energy impinges on the upper face of the collector plate. A part of the total solar radiation falls on the upper surface of the flow channels, while another part is incident on the plates connecting any two adjacent flow channels. The latter is conducted in a transverse direction toward the flow channels. The temperature is a maximum at any midpoint between adjacent channels, and the collector plate acts as a fin attached to the walls of the flow channel. The thermal performance of a fin can be expressed in terms of its efficiency. The fin efficiency η_f is defined as the ratio of the rate of heat flow through the real fin to the rate of heat flow through a fin of infinite thermal conductivity, that is, a fin at a uniform temperature. We shall now derive a relation to evaluate this efficiency for a flat-plate solar collector.

If U_c is the overall unit conductance from the collector-plate surface to the ambient air, the rate of heat loss from a given segment of the collector plate at x,y in Fig. 3.14 is

$$q(x,y) = U_c[T_c(x,y) - T_a]dxdy, \tag{3.24}$$

where T_c = local collector-plate temperature ($T_c > T_a$)
T_a = ambient air temperature
U_c = overall unit conductance between the plate and the ambient air

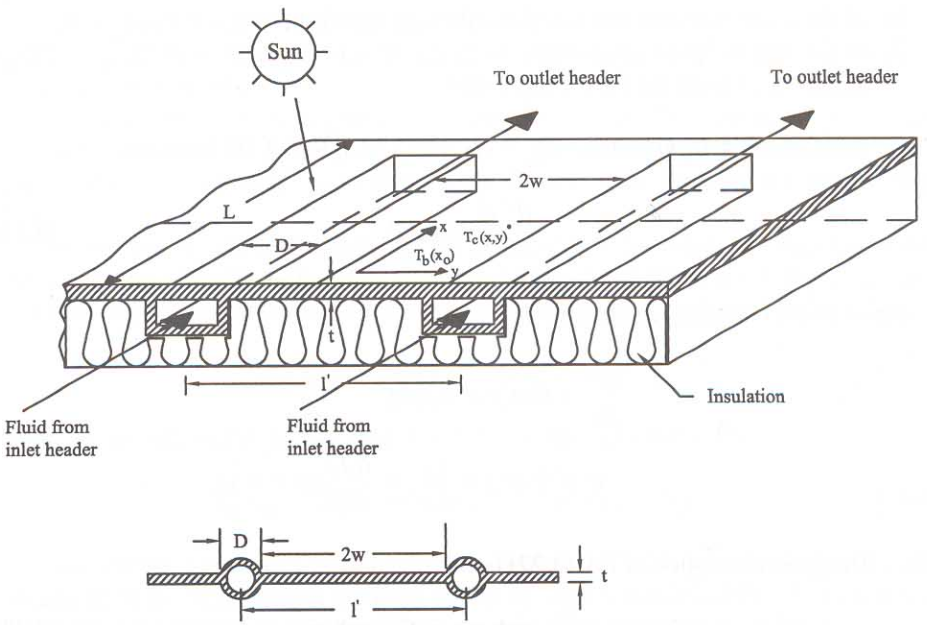

Figure 3.14. Sketch showing coordinates and dimensions for collector plate and fluid ducts.

U_c includes the effects of radiation and free convection between the plates, the radiative and convective transfer between the top of the cover and the environment, and conduction through the insulation. Its quantitative evaluation has been previously considered.

If conduction in the x direction is negligible, a heat balance at a given distance x_0 for a cross section of the flat-plate collector per unit length in the x direction can be written in the form

$$\alpha_s I_s dy - U_c(T_c - T_a)dy + \left(-kt\frac{dT_c}{dy}\bigg|_{y,x_0}\right) - \left(-kt\frac{dT_c}{dy}\bigg|_{y+dy,x_0}\right) = 0. \quad (3.25)$$

If the plate thickness t is uniform and the thermal conductivity of the plate is independent of temperature, the last term in Eq. (3.25) is

$$\frac{dT_c}{dy}\bigg|_{y+dy,x_0} = \frac{dT_c}{dy}\bigg|_{y,x_0} + \left(\frac{d^2T_c}{dy^2}\right)_{y,x_0} dy,$$

and Eq. (3.25) can be cast into the form of a second-order differential equation:

$$\frac{d^2T_c}{dy^2} = \frac{U_c}{kt}\left[T_c - \left(T_a + \frac{\alpha_s I_s}{U_c}\right)\right] \quad (3.26)$$

The boundary conditions for the system described above at a fixed x_0, are:

1. At the center between any two ducts the heat flow is 0, or at $y = 0$, $dT_c = 0$.
2. At the duct the plate temperature is $T_b(x_0)$, or at $y = w = (l' - D)/2$, $T_c = T_b(x_0)$, where $T_b(x_0)$ is the fin-base temperature.

If we let $m^2 = U_c/kt$ and $\phi = T_c - (T_a + \alpha_s I_s/U_c)$, Eq. (3.26) becomes

$$\frac{d^2\phi}{dy^2} = m^2\phi, \quad (3.27)$$

subject to the boundary conditions

$$\frac{d\phi}{dy} = 0 \text{ at } y = 0, \text{ and}$$

$$\phi = T_b(x_0) - \left(T_a + \frac{\alpha_s I_s}{U_c}\right) \text{ at } y = w.$$

The general solution of Eq. (3.27) is

$$\phi = C_1 \sinh my + C_2 \cosh my. \quad (3.28)$$

The constants C_1 and C_2 can be determined by substituting the two boundary conditions and solving the two resulting equations for C_1 and C_2. This gives

$$\frac{T_c - (T_a + \alpha_s I_s/U_c)}{T_b(x_0) - (T_a + \alpha_s I_s/U_c)} = \frac{\cosh my}{\cosh mw}. \tag{3.29}$$

From the preceding equation the rate of heat transfer to the conduit from the portion of the plate between two conduits can be determined by evaluating the temperature gradient at the base of the fin, or

$$q_{fin} = -kt\frac{dT_c}{dy}\bigg|_{y=w} = \frac{1}{m}\{\alpha_s I_s - U_c[T_b(x_0) - T_a]\tanh mw\}. \tag{3.30}$$

Since the conduit is connected to fins on both sides, the total rate of heat transfer is

$$q_{total}(x_0) = 2w\{\alpha_s I_s - U_c[T_b(x_0) - T_a]\}\frac{\tanh mw}{mw}. \tag{3.31}$$

If the entire fin were at the temperature $T_b(x_0)$, a situation corresponding physically to a plate of infinitely large thermal conductivity, the rate of heat transfer would be a maximum, $q_{total,max}$. As mentioned previously, the ratio of the rate of heat transfer with a real fin to the maximum rate obtainable is the fin efficiency η_f. With this definition, Eq. (3.31) can be written in the form

$$q_{total}(x_0) = 2w\eta_f\{\alpha_s I_s - U_c[T_b(x_0) - T_a]\}, \tag{3.32}$$

where $\eta_f \equiv \tanh mw/mw$.

The fin efficiency η_f is plotted as a function of the dimensionless parameter $w(U_c/kt)^{1/2}$ in Fig. 3.15. When the fin efficiency approaches unity, the maximum portion of the radiant energy impinging on the fin becomes available for heating the fluid.

In addition to the heat transferred through the fin, the energy impinging on the portion of the plate above the flow passage is also useful. The rate of useful energy from this region available to heat the working fluid is

$$q_{duct}(x_0) = D\{a_s I_s - U_c[T_b(x_0) - T_a]\}. \tag{3.33}$$

Thus, the useful energy per unit length in the flow direction becomes

$$q_u(x_0) = (D + 2w\eta)\{\alpha_s I_s - U_c[T_b(x_0) - T_a]\}. \tag{3.34}$$

The energy $q_u(x_0)$ must be transferred as heat to the working fluid. If the thermal resistance of the metal wall of the flow duct is negligibly small and there is no contact resistance between the duct and the plate, the rate of heat transfer to the fluid is

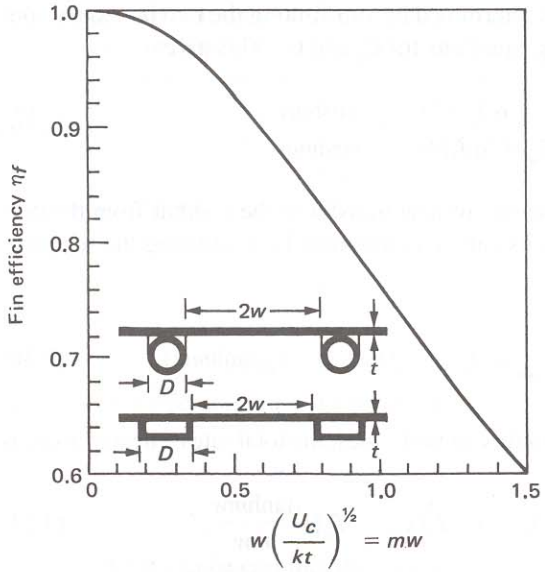

Figure 3.15. Fin efficiency for tube and sheet flat-plate solar collectors.

$$q_u(x_0) = P\bar{h}_{c,i}[T_b(x_0) - T_f(x_0)], \tag{3.35}$$

where P is the perimeter of the flow duct, which is $2(D + d)$ for a rectangular duct. Contact resistance may become important in poorly manufactured collectors in which the flow duct is clamped or glued to the collector plate. Collectors manufactured by such methods are usually not satisfactory.

3.2.6 Collector Efficiency Factor

To obtain a relation for the useful energy delivered by a collector in terms of known physical parameters, the fluid temperature, and the ambient temperature, the collector temperature must be eliminated from Eqs. (3.34) and (3.35). Solving for $T_b(x_0)$ in Eq. (3.35) and substituting this relation in Eq. (3.34) gives

$$q_u(x_0) = l'F'\{\alpha_s I_s - U_c[T_f(x_0) - T_a]\}, \tag{3.36}$$

where F′ is called the collector efficiency factor [9], and $l' = (2w+D)$. F' is given by

$$F' = \frac{1/U_c}{l'[1/(U_c(D + 2w\eta_f)) + 1/(\bar{h}_{c,i}P)]}. \tag{3.37}$$

For a flow duct of circular cross section of diameter D, F' can be written as

Table 3.6. Typical values for the parameters that determine the collector efficiency factor F' for a flat-plate collector in Eq. (3.37).

		U_c
2 glass covers	4 W/m² · K	0.685 Btu/hr · ft² · °F
1 glass cover	8 W/m² · K	1.37 B Btu/hr · ft² · °F
		kt
copper plate, 1 mm thick	0.38 W/K	0.72 Btu/hr · °F
steel plate, 1 mm thick	0.045 W/K	0.0866 Btu/hr · °F
		$\bar{h}_{c,i}$
water in laminar flow forced convection	300 W/m² · K	52 Btu/hr · ft² · °F
water in turbulent flow forced convection	1500 W/m² · K	254 Btu/hr · ft² · °F
air in turbulent forced convection	100 W/m² · K	17.6 Btu/hr · ft² · °F

$$F' = \frac{1/U_c}{l'[1/(U_c(D + 2w\eta_f)) + 1/(\bar{h}_{c,i}\pi D)]}$$

Physically, the denominator in Eq. (3.37) is the thermal resistance between the fluid and the environment, whereas the numerator is the thermal resistance between the collector surface and the ambient air. The collector-plate efficiency factor F' depends on U_c, $\bar{h}_{c,i}$, and η_f. It is only slightly dependent on temperature and can, for all practical purposes, be treated as a design parameter. Typical values for the factors determining the value of F' are given in Table 3.6.

The collector efficiency factor increases with increasing plate thickness and plate thermal conductivity, but it decreases with increasing distance between flow channels. Also, increasing the heat-transfer coefficient between the walls of the flow channel and the working fluid increases F', but an increase in the overall conductance U_c will cause F' to decrease.

3.2.7 Collector Heat-Removal Factor

Equation (3.36) yields the rate of heat transfer to the working fluid at a given point x along the plate for specified collector and fluid temperatures. However, in a real collector the fluid temperature increases in the direction of flow as heat is transferred to it. An energy balance for a section of flow duct dx can be written in the form

$$\dot{m}c_p(T_f|_{x+dx} - T_f|_x) = q_u(x)dx. \tag{3.38}$$

Substituting Eq. (3.36) for $q_u(x)$ and $T_f(x) + (dT_f(x)/dx)\,dx$ for $T_f|_{x+dx}$ in Eq. (3.38) gives the differential equation

$$\dot{m}c_p\frac{dT_f(x)}{dx} = l'F'\{\alpha_s I_s - U_c[T_f(x) - T_a]\}. \tag{3.39}$$

Separating the variables gives, after some rearranging,

$$\frac{dT_f(x)}{T_f(x) - T_a - \alpha_s I_s/U_c} = \frac{l'F'U_c}{\dot{m}c_p}dx. \tag{3.40}$$

Equation (3.40) can be integrated and solved for the outlet temperature of the fluid $T_{f,out}$ for a duct length L, and for the fluid inlet temperature $T_{f,in}$ if we assume that F′ and U_c are constant, or

$$\frac{T_{f,out} - T_a - \alpha_s I_s/U_c}{T_{f,in} - T_a - \alpha_s I_s/U_c} = \exp\left(-\frac{U_c l'F'L}{\dot{m}c_p}\right). \tag{3.41}$$

To compare the performance of a real collector with the thermodynamic optimum, it is convenient to define the heat-removal factor F_R as the ratio between the actual rate of heat transfer to the working fluid and the rate of heat transfer at the minimum temperature difference between the absorber and the environment.

The thermodynamic limit corresponds to the condition of the working fluid remaining at the inlet temperature throughout the collector. This can be approached when the fluid velocity is very high. From its definition F_R can be expressed as

$$F_R = \frac{Gc_p(T_{f,out} - T_{f,in})}{\alpha_s I_s - U_c(T_{f,in} - T_a)}, \tag{3.42}$$

where G is the flow rate per unit surface area of collector $\dot{m}/A_c$. By regrouping the right-hand side of Eq. (3.42) and combining with Eq. (3.41), it can easily be verified that

$$\begin{aligned} F_R &= \frac{Gc_p}{U_c}\left[1 - \frac{\alpha_s I_s/U_c - (T_{f,out} - T_a)}{\alpha_s I_s/U_c - (T_{f,in} - T_a)}\right] \\ &= \frac{Gc_p}{U_c}\left[1 - \exp\left(-\frac{U_c F'}{Gc_p}\right)\right]. \end{aligned} \tag{3.43}$$

Inspection of the above relation shows that F_R increases with increasing flow rate and approaches as an upper limit F′, the collector efficiency factor. Since the numerator of the right-hand side of Eq. (3.42) is q_u, the rate of useful heat transfer can now be expressed in terms of the fluid inlet temperature, or

$$q_u = A_c F_R[\alpha_s I_s - U_c(T_{f,in} - T_a)]. \tag{3.44}$$

If a glazing above the absorber plate has transmittance τ_s then

$$q_u = A_c F_R[\tau_s \alpha_s I_c - U_c(T_{f,in} - T_a)], \tag{3.45}$$

and instantaneous efficiency η_c is

$$\eta_c = \frac{q_u}{I_c A_c} = F_R[\tau_s \alpha_s - U_c(T_{f,in} - T_a)/I_c] \tag{3.46}$$

Equation (3.46) is also known as the ***Hottel-Whillier-Bliss*** equation. This is a convenient form for design, because the fluid inlet temperature to the collector is usually known or can be specified.

Example 3.1. Calculate the averaged hourly and daily efficiency of a water solar collector on January 15, in Boulder, CO. The collector is tilted at an angle of 60° and has an overall conductance of 8.0 W/m² · K on the upper surface. It is made of copper tubes, with a 1-cm ID, 0.05 cm thick, which are connected by a 0.05-cm-thick plate at a center-to-center distance of 15 cm. The heat-transfer coefficient for the water in the tubes is 1500 W/m² · K, the cover transmittance is 0.9, and the solar absorptance of the copper surface is 0.9. The collector is 1 m wide and 2 m long, the water inlet temperature is 330 K, and the water flow rate is 0.02 kg/sec. The horizontal insolation (total) I_h and the environmental temperature are tabulated below. Assume the diffuse radiation accounts for 25 percent of the total insolation.

Solution. The total radiation received by the collector is calculated from Eq. (2.42) and neglecting the ground reflected radiation:

$$I_c = I_{d,c} + I_{b,c} = 0.25 I_h \cos^2\left(\frac{60}{2}\right) + (1 - 0.25) I_h R_b.$$

Time (hr)	I_h (W/m²)	T_{amb} (K)
7–8	12	270
8–9	80	280
9–10	192	283
10–11	320	286
11–12	460	290
12–13	474	290
13–14	395	288
14–15	287	288
15–16	141	284
16–17	32	280

The tilt factor R_b is obtained from its definition in Chapter 2 [see Eq. (2.58)]:

$$R_b = \frac{\cos i}{\sin \alpha} = \frac{\sin(L - \beta)\sin\delta_s + \cos(L - \beta)\cos\delta_s \cos h_s}{\sin L \sin\delta_s + \cos L \cos\delta_s \cos h_s}$$

where L = 40° δ_s = −21.1 on January 15 (from Fig. 2.8), and β = 60°. The hour angle h_s equals 15° for each hour away from noon.

The fin efficiency is obtained from Eq. (3.32):

$$\eta_f = \frac{\tanh m(l' - D)/2}{m(l' - D)/2}$$

where

$$m = \left(\frac{U_c}{kt}\right)^{1/2} = \left(\frac{8}{390 \times 5 \times 10^{-4}}\right)^{1/2} = 6.4, \text{ and}$$

$$\eta_f = \frac{\tanh 6.4(0.15 - 0.01)/2}{6.4(0.15 - 0.01)/2} = 0.938.$$

The collector efficiency factor F′ is, from Eq. (3.37),

$$F' = \frac{1/U_c}{l'[1/(U_c(D + 2w\eta_f)) + 1/(h_{c,i}\pi D)]}$$

$$= \frac{1/8.0}{0.15[1/8.0(0.01 + 0.14 \times 0.938) + 1/1500\pi \times 0.01]} = 0.92.$$

Then we obtain the heat-removal factor from Eq. (3.43):

$$F_R = \frac{Gc_p}{U_c}\left[1 - \exp\left(-\frac{U_c F'}{Gc_p}\right)\right].$$

Time (hr)	I_h (W/m²)	R_b	$I_{d,c}$ (W/m²)	$I_{b,c}$ (W/m²)	I_c (W/m²)	q_u (W)	T_{amb} (K)	η_c
7–8	12	10.9	1	98	99	0	270	0
8–9	80	3.22	5	193	198	0	280	0
9–10	192	2.44	12	351	363	0	283	0
10–11	320	2.18	20	523	543	148	286	0.137
11–12	460	2.08	29	718	747	482	290	0.322
12–13	474	2.08	30	739	769	512	290	0.333
13–14	395	2.18	25	646	671	351	288	0.261
14–15	287	2.49	18	525	543	175	288	0.162
15–16	141	3.22	9	341	350	0	284	0
16–17	32	10.9	2	261	263	0	280	0

$$F_R = \frac{0.01 \times 4184}{8.0}\left[1 - \exp\left(-\frac{8.0 \times 0.922}{0.01 \times 4184}\right)\right] = 0.845.$$

From Eq. (3.45), the useful heat delivery rate is

$$q_u = 2 \times 0.845[I_c \times 0.81 - 8.0(T_{f,in} - T_{amb})].$$

The efficiency of the collector is $\eta_c = q_u / A_c I_c$ and the hourly averages are calculated in the table above.

Thus, $\Sigma I_c = 4546$ W/m^2 and $\Sigma q_u = 1668$W. The daily average efficiency is obtained by summing the useful energy for those hours during which the collector delivers heat and dividing by the total insolation between sunrise and sunset. This yields

$$\overline{\eta}_{c,day} = \frac{\Sigma q_u}{\Sigma A_c I_c} = \frac{1668}{2 \times 4546} = 0.183 \text{ or } 18.3 \text{ percent}$$

3.2.8 Transient Effects

The preceding analysis assumed that steady-state conditions exist during the operation of the collector. Under actual operating conditions the rate of insolation will vary and the ambient temperature and the external wind conditions may change. To determine the effect of changes in these parameters on the performance of a collector it is necessary to make a transient analysis that takes the thermal capacity of the collector into account.

As shown in [42], the effect of collector thermal capacitance is the sum of two contributions: the ***collector storage*** effect, resulting from the heat required to bring the collector up to its final operating temperature, and the ***transient*** effect, resulting from fluctuations in the meteorological conditions. Both effects result in a net loss of energy delivered compared with the predictions from the zero capacity analsysis. This loss is particularly important on a cold morning when all of the solar energy absorbed by the collector is used to heat the hardware and the working fluid, thus delaying the delivery of useful energy for some time after the sun has come up.

Transient thermal analyses can be made with a high degree of precision [47], but the analytical predictions are no more accurate than the weather data and the overall collector conductance. For most engineering applications, a simpler approach is therefore satisfactory [19]. For this approach, it will be assumed that the absorber plate, the ducts, the back insulation, and the working fluid are at the same temperature. If back losses are neglected, an energy balance on the collector plate and the working fluid for a single-glazed collector delivering no useful energy can be written in the form

$$(\overline{mc})_p \frac{d\overline{T}_p(t)}{dt} = A_c I_s \alpha_s + A_c U_p[\overline{T}_g(t) - \overline{T}_p(t)], \tag{3.47}$$

where $(\overline{mc})_p$ is the sum of the thermal capacities of the plate, the fluid, and the insolation, I_s is the insolation on the absorber plate, and U_p is the conductance between the

air-conditioning system. The magnitude of the reduction in heating system operation will be described in the next section.

5.1.3 The Degree-day Method

The preceding analysis of heat loss from buildings expresses the loss on a per unit temperature difference basis (except for unexposed floor slabs). In order to calculate the peak load and total annual load for a building, appropriate design temperatures must be defined for each. The outdoor design temperature is usually defined statistically, such that the actual outdoor temperature will exceed the design temperature 97.5 or 99 percent of the time over a long period. The design temperature difference (ΔT) is then the interior building temperature minus the outdoor design temperature. The design ΔT is used for rating nonsolar heating systems, but is not useful for selection of solar systems, since solar systems rarely provide 100 percent of the energy demand of a building at peak conditions.

A more useful index of heating energy demand is the total annual energy requirement for a building. This quantity is somewhat more difficult to calculate than the peak load. It requires a knowledge of day-to-day variations in ambient temperature during the heating season and the corresponding building heat load for each day. Building heat loads vary with ambient temperatures as shown in Fig. 5.3. The environmental

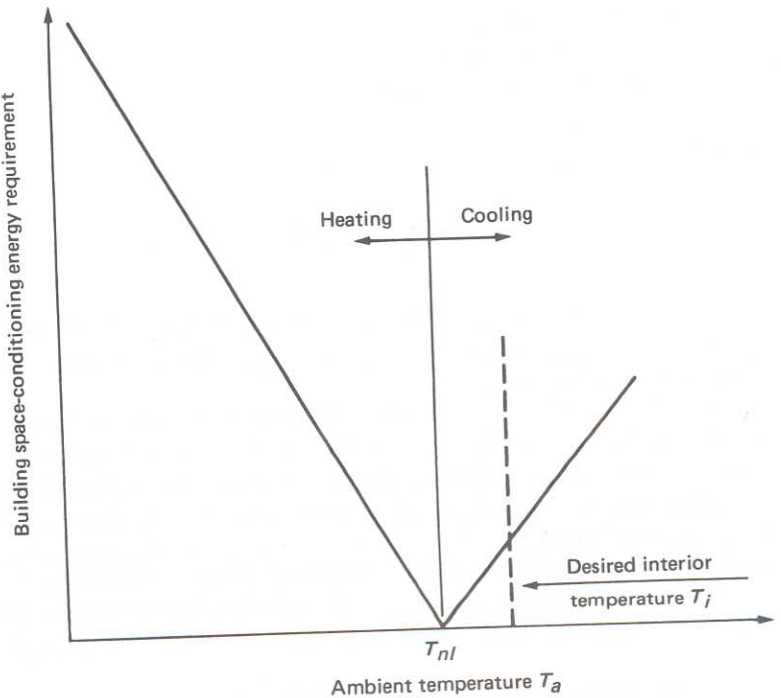

Figure 5.3. Building load profile versus ambient temperature showing no-load temperature T_{nl} and desired interior temperature T_i.

temperature T_{nl}, above which no heat need be supplied to the building, is a few degrees below the required interior temperature T_i because of internal heat-generation effects.

The no-load temperature at which internal source generation q_i just balances transmission and infiltration losses can be determined from the energy balance

$$q_i = \overline{UA}(T_i - T_{nl}), \tag{5.5}$$

where $\overline{UA}$ is the overall loss coefficient for the building (W/°C). Then

$$T_{nl} = T_i - \frac{q_i}{\overline{UA}} \tag{5.6}$$

The total annual heat load on the building, Q_T, can be expressed as

$$Q_T = \int_{365 \text{ days}} \overline{UA}(T_{nl} - T_a)^+ \, dt, \tag{5.7}$$

in which all arguments of the integral are functions of time. The superscript $^+$ indicates that only positive values are considered. In practice, it is difficult to evaluate this integral; therefore, three simplifying assumptions are made:

1. $\overline{UA}$ is independent of time.
2. T_{nl} is independent of time.
3. The integral can be expressed by the sum.

Thus,

$$\overline{UA} \sum_{n=1}^{365} (T_{nl} - \overline{T}_a)_n^+ \tag{5.8}$$

where n is the day number, and the daily average temperature $\overline{T}_a$ can be approximated by $\frac{1}{2}(T_{a,\max} + T_{a,\min})$, in which $T_{a,\max}$ and $T_{a,\min}$ are the daily maximum and minimum temperatures, respectively.

The quantity $(T_{nl} - \overline{T}_a)^+$ is called the ***degree-day unit***. For example, if the average ambient temperature for a day is 5°C and the no-load temperature is 20°C, 15 degree C-days are said to exist for that day. However, if the ambient temperature is 20°C or higher, 0 degree-days exist, indicating 0 demand for heating that day. Degree-day totals for monthly ($\Sigma_{month}\,(T_{nl} - \overline{T}_a)^+$) and annual periods can be used directly in Eq. (5.8) to calculate the monthly and annual heating energy requirements.

In the past, a single value of temperature has been used throughout the United States as a universal degree-day base, 65.0°F or 18.3°C.* This practice is now out-

*The degree-day base in SI units is defined as 19.0°C, not 18.3°C, which corresponds to 65.0°F. Therefore, precise conversion between the two systems is not possible by a simple multiplication by 5/9.

dated, since many homeowners and commercial building operators have lowered their thermostat settings in response to increased heating fuel costs, thereby lowering T_{nl}. Likewise, warehouses and factories operate well below the 19°C level. Therefore, a more generalized database of degree-days to several bases (values of T_{nl}) has been created by the U.S. National Weather Service (NWS).

Thom [32–34], in a series of papers, developed a statistically rigorous method of calculating degree-days to any base from values of ambient temperature and monthly standard deviations of ambient temperature. The details of this method are too lengthy to present here. However, the NWS has used this method to prepare tabulations of degree F-days for many U.S. locations. In addition, maps of degree F-days to the standard base are available on a monthly basis [35].

A variable base degree-day method, which recognizes that T_{nl} may vary not only with location but also from building to building, is more accepted now [3, 9, 12, 25]. Kreider and Rabl [25] have described this method in detail. Erbs et al. [12] developed a model to estimate variable base degree-days that needs as input only $\overline{T}_a$ for each month. Balcomb et al. [3] have listed monthly degree-days to bases of 50°F, 55°F, 60°F, 65°F, and 70°F for 209 U.S. and Canadian cities.

Example 5.2. A building located in Denver, CO, has a heat-loss coefficient $\overline{UA}$ of 1000 kJ/hr · °C and internal heat sources of 4440 kJ/hr. If the interior temperature is 20°C (68°F), what are the monthly and annual heating energy requirements? A gas furnace with 65 percent efficiency is used to heat the building.

Solution. In order to determine the monthly degree-day totals, the no-load temperature (degree-day basis) must be evaluated from Eq. (5.6).

$$T_{nl} = 20 - \frac{4440}{1000} = 15.6°\,C(60°\,F)$$

The monthly degree C-days for Denver are taken from the U.S. National Weather Service and given in Table 5.3. The energy demand is calculated as

$$\text{Energy Demand} = \overline{UA} \times 24\frac{\text{hr}}{\text{day}} \times \text{Degree C} - \text{days}. \tag{5.9}$$

The monthly energy demand is given in Table 5.3.

The annual energy demand of 62.9 GJ is delivered by a 65 percent efficient device. Therefore,

$$\text{Average Annual Purchased Energy} = \frac{62.9}{0.65}\text{GJ} = 96.8\text{ GJ}.$$

Table 5.3. Monthly and annual energy demands for Example 5.2.

Month	Degree C-days	Energy demand[a] (GJ)
Jan.	518	12.4
Feb.	423	10.2
Mar.	396	9.5
Apr.	214	5.2
May	68	1.6
June	14	0.3
July	0	0
Aug.	0	0
Sep.	26	0.6
Oct.	148	3.6
Nov.	343	8.2
Dec.	472	11.3
Total	2622	62.9

[a]Energy demand equals $\overline{UA}$ × degree C-days × 24 hrs/day.

5.1.4 Service Hot-Water Load Calculation

Service hot-water loads can be calculated precisely with the knowledge of only a few variables. The data required for calculation of hot-water demand are

Water source temperature (T_s)
Water delivery temperature (T_d)
Volumetric demand rate (Q)

The energy requirement for service water heating q_{hw} is given by

$$q_{hw}(t) = \rho_w Q(t) c_{pw} [T_d - T_s(t)], \tag{5.10}$$

where ρ_w is the water density and c_{pw} is its specific heat. The demand rate, $Q(t)$, varies in general with time of day and time of year; likewise, the source temperature varies seasonally. Source temperature data are not compiled in a single reference; local water authorities are the source of such temperature data.

Few generalized data exist with which to predict the demand rate Q. Table 5.4 indicates some typical usage rates for several common building types. Process water heating rates are peculiar to each process and can be ascertained by reference to process specifications.

Example 5.3. Calculate the monthly energy required to heat water for a family of four in Nashville, TN. Monthly source temperatures for Nashville are shown in Table 5.5, and the water delivery temperature is 60°C (140°F).

Table 5.4. Approximate service hot-water demand rates

	Demand per person	
Usage type	liters/day	gal/day
Retail store	2.8	0.75
Elementary school	5.7	1.5
Multifamily residence	76.0	20.0
Single-family residence	76.0	20.0
Office building	11.0	3.0

Solution. For a family of four, the demand rate Q may be found using a demand recommended from Table 5.4:

$$Q = 4 \times 76 \text{ liters/day} = 0.30 \text{ m}^3\text{/day}$$

The density of water can be taken as 1000 kg/m^3 and the specific heat as 4.18 kJ/kg · °C.

Monthly demands are given by

$$\begin{aligned} q_m &= (Q \times \text{days/month})(\rho_w c_{pw})[T_d - T_s(t)] \\ &= (0.30 \times \text{days/month})(1000 \times 4.18)[60 - T_s(t)]. \end{aligned}$$

The monthly energy demands calculated from the equation above with these data are tabulated in Table 5.5.

Table 5.5. Water heating energy demands for Example 5.3.

Month	Days/month	Demand (m^3/month)	Source temperature C°	Energy requirement (GJ/month)
Jan.	31	9.3	8	2.0
Feb.	28	8.4	8	1.8
Mar.	31	9.3	12	1.9
Apr.	30	9.0	19	1.5
May	31	9.3	17	1.7
June	30	9.0	21	1.5
July	31	9.3	22	1.5
Aug.	31	9.3	24	1.4
Sep.	30	9.0	24	1.4
Oct.	31	9.3	22	1.5
Nov.	30	9.0	14	1.7
Dec.	31	9.3	12	1.9

5.2 SOLAR WATER HEATING SYSTEMS

Solar water-heating systems represent the most common application of solar energy at the present time. Small systems are used for domestic hot water applications while larger systems are used in industrial process heat applications. There are basically two types of water-heating systems: ***natural circulation*** or passive solar system (thermosyphon) and ***forced circulation*** or active solar system. Natural circulation solar water heaters are simple in design and low cost. Their application is usually limited to nonfreezing climates, although they may also be designed with heat exchangers for mild freezing climates. Forced circulation water heaters are used in freezing climates and for commercial and industrial process heat.

5.2.1 Natural Circulation Systems

The natural tendency of a less dense fluid to rise above a denser fluid can be used in a simple solar water heater to cause fluid motion through a collector [10]. The density difference is created within the solar collector where heat is added to the liquid. In the system shown in Fig. 5.4, as water gets heated in the collector, it rises to the tank, and the cooler water from the tank moves to the bottom of the collector, setting up a natural circulation loop. It is also called a ***thermosyphon loop.*** Since this water heater does not use a pump, it is a passive water heater. For the thermosyphon to work, the storage tank must be located higher than the collector.

The flow pressure drop in the fluid loop (ΔP_{FLOW}) must equal the bouyant force "pressure difference" ($\Delta P_{BOUYANT}$) caused by the differing densities in the hot and cold legs of the fluid loop:

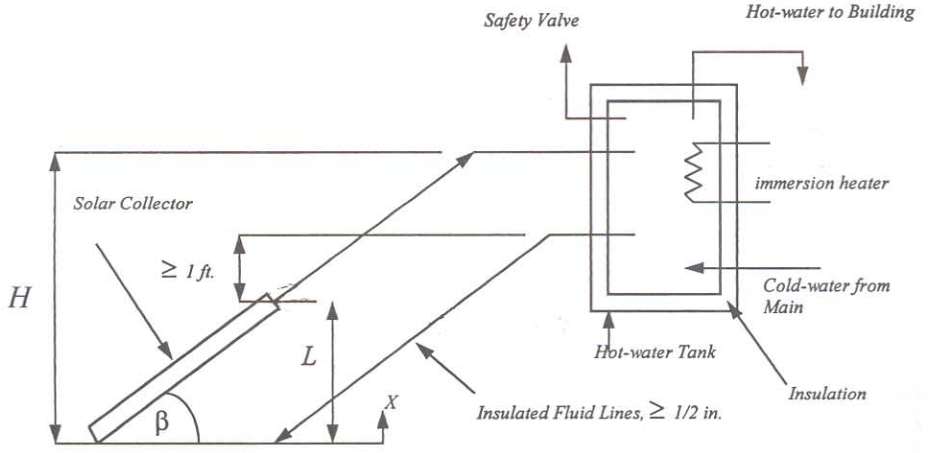

Figure 5.4. Schematic diagram of thermosyphon loop used in a natural circulation, service water-heating system. The flow pressure drop in the fluid loop must equal the bouyant force "pressure" $\left[\int_o^L g\rho(x)dx - \rho_{stor}gL\right]$ where $\rho(x)$ is the local collector fluid density and ρ_{stor} is the tank fluid density, assumed uniform.

$$\Delta P_{FLOW} = \Delta P_{BOUYANT}$$
$$= \rho_{stor} gH - \left[\int_o^L \rho(x) g dx + \rho_{out} g(H - L) \right], \tag{5.11}$$

where H is the height of the legs and L the height of the collector (see Fig. 5.4), $\rho(x)$ is the local collector fluid density, ρ_{stor} is the tank fluid density, and ρ_{out} is the collector outlet fluid density, the latter two densities assumed uniform. The flow pressure term ΔP_{FLOW}, is related to the flow loop system head loss, which is in turn directly connected to friction and fitting losses and the loop flow rate:

$$\Delta P_{FLOW} = \oint_{LOOP} \rho d(h_L), \tag{5.12}$$

where $h_L = KV^2$, with K being the sum of the component loss velocity factors (see any fluid mechanics text) and V the flow velocity.

Since the driving force in a thermosyphon system is only a small density difference and not a pump, larger-than-normal plumbing fixtures must be used to reduce pipe friction losses [30]. In general, one pipe size larger than normal would be used with a pump system is satisfactory. Figure 5.5 shows some passive water heaters.

Since the hot-water system loads vary little during a year, the angle of tilt is that equal to the latitude, that is, $\beta = L$. The temperature difference between the collector inlet water and the collector outlet water is usually 8–11°C during the middle of a sunny day [10]. After sunset, a thermosyphon system can reverse its flow direction and lose heat to the environment during the night. To avoid reverse flow, the top header of the absorber should be at least 30 cm below the cold leg fitting on the storage tank, as shown, otherwise a check valve would be needed.

To provide heat during long cloudy periods, an electrical immersion heater can be used as a backup for the solar system. The immersion heater is located near the top of the tank to enhance stratification and so that the heated fluid is at the required delivery temperature. Tank stratification is desirable in a thermosyphon to maintain flow rates as high as possible. Insulation must be applied over the entire tank surface to control heat loss.

Several features inherent in the thermosyphon design limit its utility. If it is to be operated in a freezing climate, a nonfreezing fluid must be used, which in turn requires a heat exchanger between collector and potable water storage. (If potable water is not required, the collector can be drained during cold periods instead.) Heat exchangers of either the shell-and-tube type or the immersion-coil type require higher flow rates for efficient operation than a thermosyphon can provide. Therefore, the thermosyphon is usually limited to nonfreezing climates. For mild freeze climates, a heat exchanger coil welded to the outer surface of the tank and filled with an antifreeze may work well.

Example 5.4. Determine the "pressure difference" available for a thermosyphon system with 1 meter high collector and 2 meter high legs. The water temperature input to the collector is 25°C and the collector output temperature is 35°C. If the overall system loss velocity factor (K) is 15.6, estimate the system flow velocity.

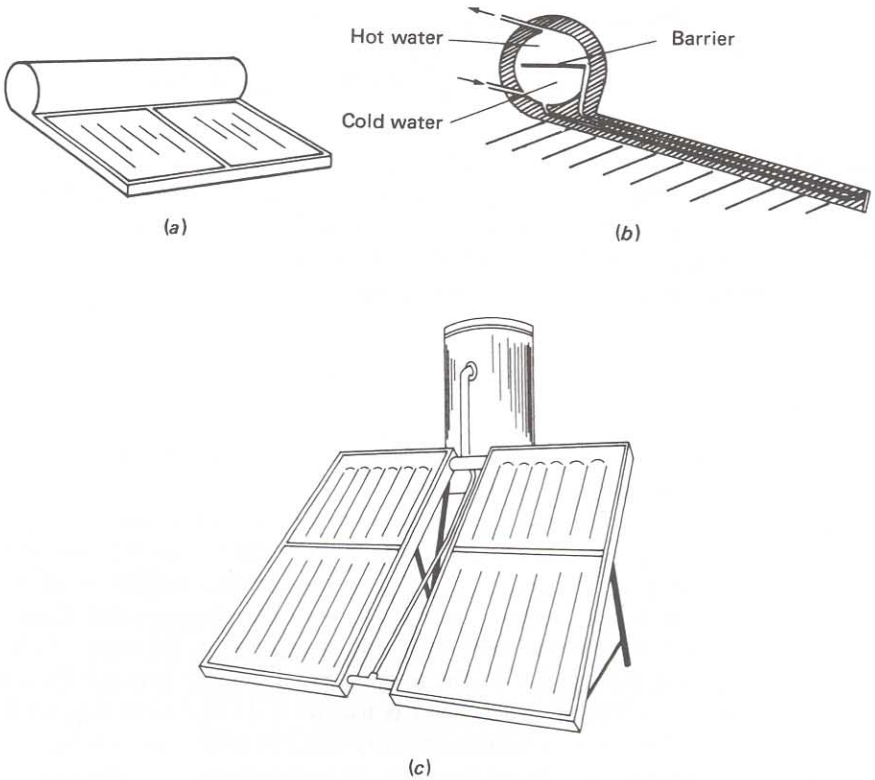

Figure 5.5. Passive solar water heaters; (a) compact model using combined collector and storage, (b) section view of the compact model, and (c) tank and collector assembly.

Solution. Equation (5.11) is used to calculate the pressure difference, with the water densities being found from the steam tables (see Appendix 3 and Tables 3.8 and 3.9).

$$\rho_{stor}(25°C) = 997.009 \text{ kg/m}^3$$

$$\rho_{out}(35°C) = 994.036 \text{ kg/m}^3$$

$\rho_{coll.ave.}(30°C) = 996.016$ kg/m^3 (note: average collector temperature used in 'integral') and with H = 2 and L = 1 m:

$$\Delta P_{BOUYANT} = (997.009)9.81(2) - [(996.016)9.81(1) + (994.036)9.81(1)]$$

$$= 38.9 \text{ N/m}^2 \text{ (Pa)}.$$

The system flow velocity is estimated from the system K given, the pressure difference calculated above, taking the average density of the water around the loop (at 30°C), and substituting into Eq. (5.12):

$$\Delta P_{BOUYANT} = (\rho_{loop.ave.})(h_L)_{loop} = (\rho_{loop.ave.})\, KV^2$$

$$V^2 = 38.9/(996.016)(15.6)$$

$$V = 0.05 \text{ m/s}$$

5.2.2 Forced-Circulation Systems

If a thermosyphon system cannot be used for climatic, structural, or architectural reasons, a forced-circulation system is required.

Figure 5.6 shows three configurations of forced circulation systems: (1) open loop, (2) closed loop, and (3) closed loop with drainback. In an open loop system (Fig. 5.6a) the solar loop is at atmospheric pressure, therefore, the collectors are empty when they are not providing useful heat. A disadvantage of this system is the high pumping power required to pump the water to the collectors every time the collectors become hot. This disadvantage is overcome in the pressurized closed loop system (Fig. 5.6b) since the pump has to overcome only the resistance of the pipes. In this system, the solar loop remains filled with water under pressure.

In order to accommodate the thermal expansion of water from heating, a small (about 2 gallon capacity) expansion tank and a pressure relief valve are provided in the solar loop. Because water always stays in the collectors of this system, antifreeze (propylene glycol or ethylene glycol) is required for locations where freezing conditions can occur. During stagnation conditions (in summer), the temperature in the col-

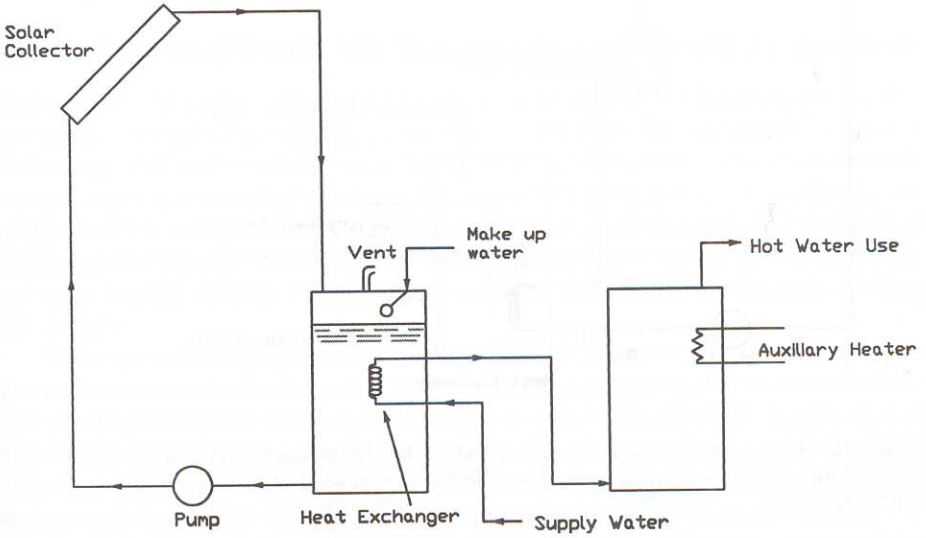

Figure 5.6. Typical configurations of solar water-heating systems: (a) open loop system.

(*continues*)

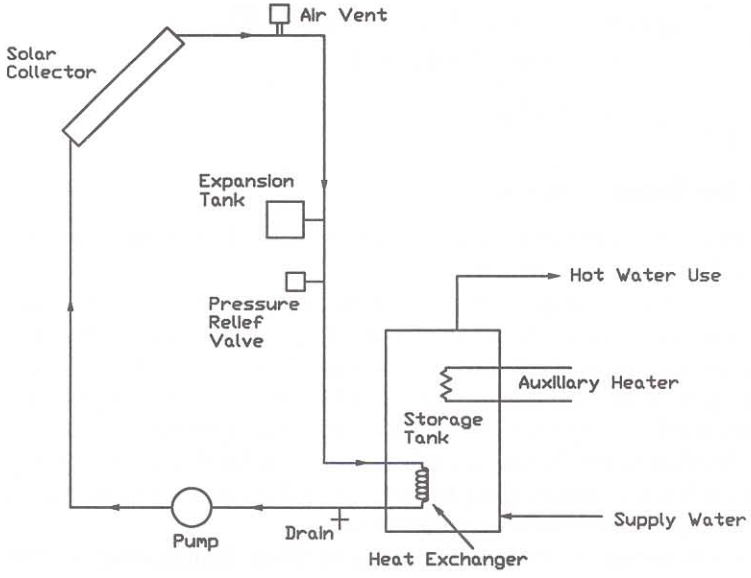

(b)

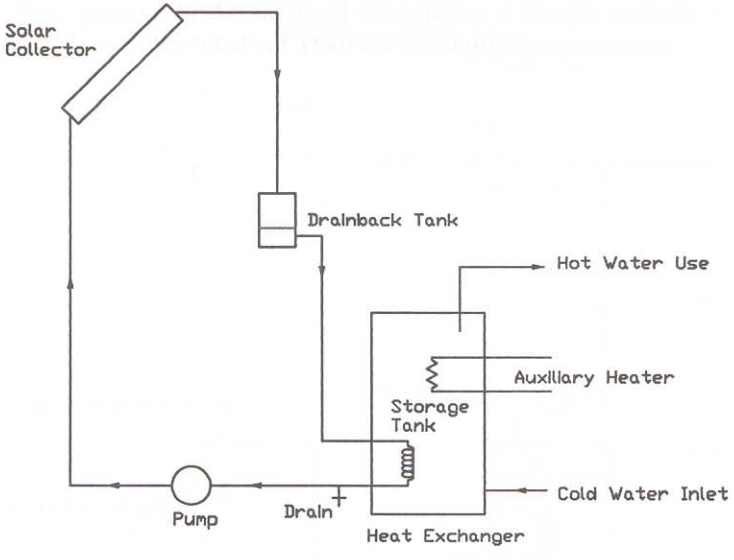

(c)

Figure 5.6. (*Continued*) (b) closed loop system; and (c) closed loop drainback system. (Adapted from Goswami, D.Y. *Alternative Energy in Agriculture*, Vol. 1. Boca Raton, FL: CRC Press, (1986).

lector can become very high, causing the pressure in the loop to increase. This can cause leaks in the loop unless some fluid is allowed to escape through a pressure-release valve. Whether the result of leaks or of draining, air enters the loop causing the pumps to run dry. This disadvantage can be overcome in a closed loop drainback system which is not pressurized (Fig. 5.6c). In this system, when the pump shuts off, the water in the collectors drains back into a small holding tank while the air in the holding tank goes up to fill the collectors. The holding tank can be located where freezing does not occur, but still at a high level to reduce pumping power. In all three configurations, a differential controller measures the temperature differential between the solar collector and the storage, and turns the circulation pump on when the differential is more than a set limit (usually 5°C) and turns it off when the differential goes below a set limit (usually 2°C). Alternatively, a photovoltaic (PV) panel and a DC pump may be used. The PV panel will turn on the pump only when solar radiation is above a minimum level. Therefore, the differential controller and the temperature sensors may be eliminated.

5.2.3 Industrial Process Heat Systems

For temperatures of up to about 100°C, required for many industrial process heat applications, forced ciculation water-heating systems described above can be used. The systems, however, will require a large collector area, storage and pumps, etc. For higher temperatures, evacuated tube collectors or concentrating collectors must be used. Industrial process heat systems are described in more detail in Chapter 8.

5.3 LIQUID-BASED SOLAR-HEATING SYSTEMS FOR BUILDINGS

The earliest active solar space-heating systems were constructed from enlarged water-heating components. Experiments beginning in 1938 at the Massachusetts Institute of Technology (MIT) showed that solar heating with liquid working fluids could be done without any major technical problems. The early MIT work formed the basis of many of the design techniques used today. Other experiments after World War II provided additional fundamental information on collector designs and storage operation for liquid-based heating systems. Fig. 5.7 shows a modern solar-heated, multifamily building in Colorado.

Solar space-heating systems can be classified as active or passive depending on the method utilized for heat transfer. A system that uses pumps and/or blowers for fluid flow in order to transfer heat is called an active system. On the other hand, a system that utilizes natural phenomena for heat transfer is called a passive system. Examples of passive solar space-heating systems include direct gain, attached greenhouse, and storage wall (also called Trombe wall). Passive solar heating systems are described in Chapter 7. In this section, configurations, design methods, and control strategies for active solar-heating systems are described.

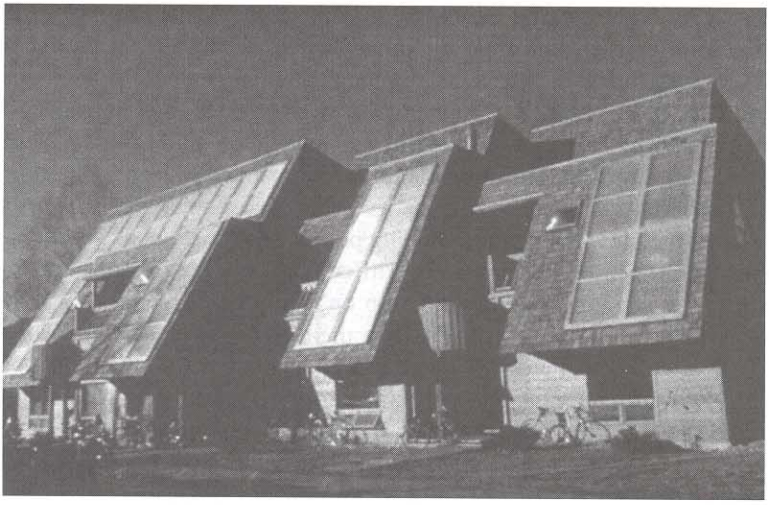

Figure 5.7. Multi-unit residence located in Boulder, CO, heated by an active solar-heating system. Courtesy of Joint Venture, Inc., Boulder, CO.

5.3.1 Physical Configurations of Active Solar Heating Systems

Figure 5.8 is a schematic diagram of a typical space-heating system. The system consists of three fluid loops–collector, storage, and load. In addition, most space-heating systems are integrated with a domestic water-heating system to improve the year long solar load factor.

Since space heating is a relatively low-temperature use of solar energy, a thermodynamic match of collector to task indicates that an efficient flat-plate collector or low-concentration solar collector is the thermal device of choice.

The collector fluid loop contains fluid manifolds, the collectors, the collector pump and heat exchanger, an expansion tank, and other subsidiary components. A collector heat-exchanger and antifreeze in the collector loop are normally used in all solar space-heating systems, since the existence of a significant heating demand implies the existence of some subfreezing weather.

The storage loop contains the storage tank and pump as well as the tube side of the collector heat exchanger. To capitalize on whatever stratification may exist in the storage tank, fluid entering the collector heat exchanger is generally removed from the bottom of storage. This strategy ensures that the lowest temperature fluid available in the collector loop is introduced at the collector inlet for high efficiency.

The energy delivery-to-load loop contains the load device, baseboard heaters or fin-and-tube coils, and the backup system with a flow control (mode selector) valve.

5.3.2 Solar Collector Orientation

The best solar collector orientation is such that the average solar incidence angle is smallest during the heating season. For tracking collectors this objective is automati-

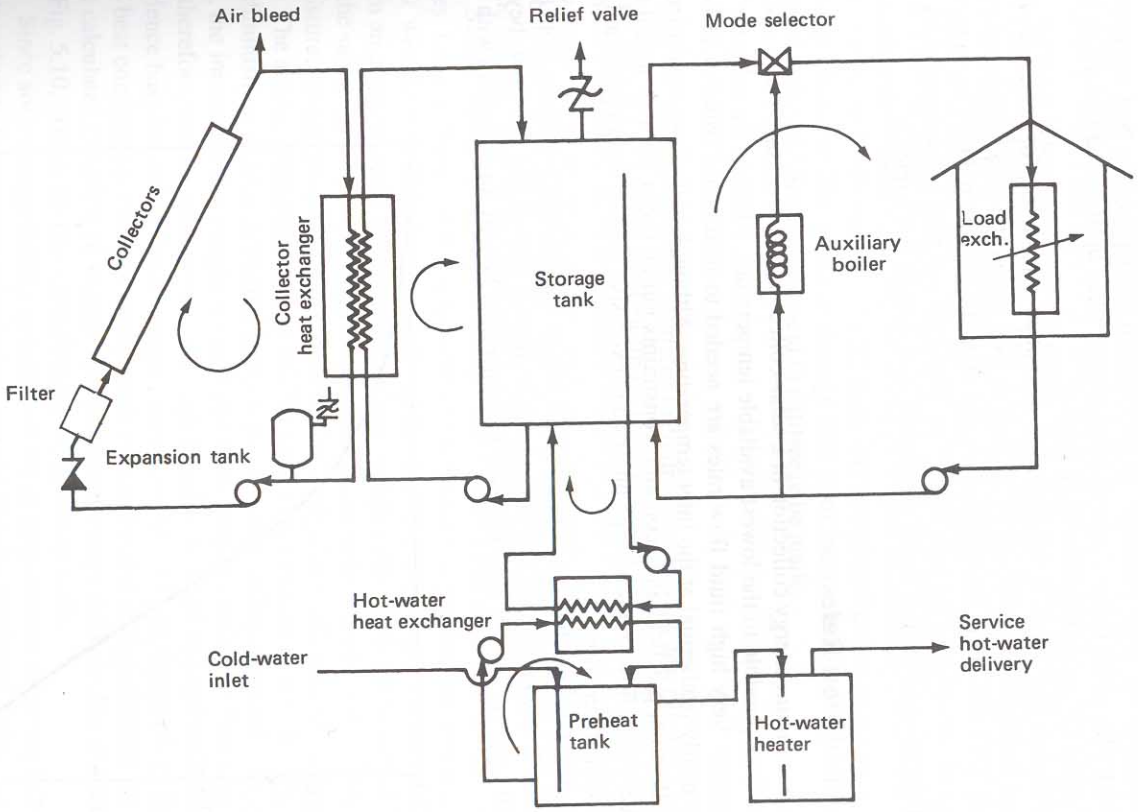

Figure 5.8. Typical solar-thermal system for space heating and hot-water heating showing fluid transport loops and pumps.

Table A2.6*a* Solar position and insolation values for 24 degrees north latitude[a]

Date	Solar time		Solar position		BTUH/sq. ft. total insolation on surface[b]						
							South facing surface angle with horiz.				
	AM	PM	Alt	Azm	Normal[c]	Horiz.	14	24	34	44	90
Jan 21	7	5	4.8	65.6	71	10	17	21	25	28	31
	8	4	16.9	58.3	239	83	110	126	137	145	127
	9	3	27.9	48.8	288	151	188	207	221	228	176
	10	2	37.2	36.1	308	204	246	268	282	287	207
	11	1	43.6	19.6	317	237	283	306	319	324	226
	12		46.0	0.0	320	249	296	319	332	336	232
	Surface daily totals				2766	1622	1984	2174	2300	2360	1766
Feb 21	7	5	9.3	74.6	158	35	44	49	53	56	46
	8	4	22.3	67.2	263	116	135	145	150	151	102
	9	3	34.4	57.6	298	187	213	225	230	228	141
	10	2	45.1	44.2	314	241	273	286	291	287	168
	11	1	53.0	25.0	321	276	310	324	328	323	185
	12		56.0	0.0	324	288	323	337	341	335	191
	Surface daily totals				3036	1998	2276	2396	2436	2424	1476
Mar 21	7	5	13.7	83.3	194	60	63	64	62	59	27
	8	4	27.2	76.8	267	141	150	152	149	142	64
	9	3	40.2	67.9	295	212	226	229	225	214	95
	10	2	52.3	54.8	309	266	285	288	283	270	120
	11	1	61.9	33.4	315	300	322	326	320	305	135
	12		66.0	0.0	317	312	334	339	333	317	140
	Surface daily totals				3078	2270	2428	2456	2412	2298	1022
Apr 21	6	6	4.7	100.6	40	7	5	4	4	3	2
	7	5	18.3	94.9	203	83	77	70	62	51	10
	8	4	32.0	89.0	256	160	157	149	137	122	16
	9	3	45.6	81.9	280	227	227	220	206	186	46
	10	2	59.0	71.8	292	278	282	275	259	237	61
	11	1	71.1	51.6	298	310	316	309	293	269	74
	12		77.6	0.0	299	321	328	321	305	280	79
	Surface daily totals				3036	2454	2458	2374	2228	2016	488
May 21	6	6	8.0	108.4	86	22	15	10	9	9	5
	7	5	21.2	103.2	203	98	85	73	59	44	12
	8	4	34.6	98.5	248	171	159	145	127	106	15
	9	3	48.3	93.6	269	233	224	210	190	165	16
	10	2	62.0	87.7	280	281	275	261	239	211	22
	11	1	75.5	76.9	286	311	307	293	270	240	34
	12		86.0	0.0	288	322	317	304	281	250	37
	Surface daily totals				3032	2556	2447	2286	2072	1800	246
Jun 21	6	6	9.3	111.6	97	29	20	12	12	11	7
	7	5	22.3	106.8	201	103	87	73	58	41	13
	8	4	35.5	102.6	242	173	158	142	122	99	16
	9	3	49.0	98.7	263	234	221	204	182	155	18
	10	2	62.6	95.0	274	280	269	253	229	199	18
	11	1	76.3	90.8	279	309	300	283	259	227	19
	12		89.4	0.0	281	319	310	294	269	236	22
	Surface daily totals				2994	2574	2422	2230	1992	1700	204

Table A2.6*a* Solar position and insolation values for 24 degrees north latitude[a] *(Continued)*

Date	Solar time		Solar position		BTUH/sq. ft. total insolation on surface[b]						
							South facing surface angle with horiz.				
	AM	PM	Alt	Azm	Normal[c]	Horiz.	14	24	34	44	90
Jul 21	6	6	8.2	109.0	81	23	16	11	10	9	6
	7	5	21.4	103.8	195	98	85	73	59	44	13
	8	4	34.8	99.2	239	169	157	143	125	104	16
	9	3	48.4	94.5	261	231	221	207	187	161	18
	10	2	62.1	89.0	272	278	270	256	235	206	21
	11	1	75.7	79.2	278	307	302	287	265	235	32
	12		86.6	0.0	280	317	312	298	275	245	36
	Surface daily totals				2932	2526	2412	2250	2036	1766	246
Aug 21	6	6	5.0	101.3	35	7	5	4	4	4	2
	7	5	18.5	95.6	186	82	76	69	60	50	11
	8	4	32.2	89.7	241	158	154	146	134	118	16
	9	3	45.9	82.9	265	223	222	214	200	181	39
	10	2	59.3	73.0	278	273	275	268	252	230	58
	11	1	71.6	53.2	284	304	309	301	285	261	71
	12		78.3	0.0	286	315	320	313	296	272	75
	Surface daily totals				2864	2408	2402	2316	2168	1958	470
Sep 21	7	5	13.7	83.8	173	57	60	60	59	56	26
	8	4	27.2	76.8	248	136	144	146	143	136	62
	9	3	40.2	67.9	278	205	218	221	217	206	93
	10	2	52.3	54.8	292	258	275	278	273	261	116
	11	1	61.9	33.4	299	291	311	315	309	295	131
	12		66.0	0.0	301	302	323	327	321	306	136
	Surface daily totals				2878	2194	2342	2366	2322	2212	992
Oct 21	7	5	9.1	74.1	138	32	40	45	48	50	42
	8	4	22.0	66.7	247	111	129	139	144	145	99
	9	3	34.1	57.1	284	180	206	217	223	221	138
	10	2	44.7	43.8	301	234	265	277	282	279	165
	11	1	52.5	24.7	309	268	301	315	319	314	182
	12		55.5	0.0	311	279	314	328	332	327	188
	Surface daily totals				2868	1928	2198	2314	2364	2346	1442
Nov 21	7	5	4.9	65.8	67	10	16	20	24	27	29
	8	4	17.0	58.4	232	82	108	123	135	142	124
	9	3	28.0	48.9	282	150	186	205	217	224	172
	10	2	37.3	36.3	303	203	244	265	278	283	204
	11	1	43.8	19.7	312	236	280	302	316	320	222
	12		46.2	0.0	315	247	293	315	328	332	228
	Surface daily totals				2706	1610	1962	2146	2268	2324	1730
Dec 21	7	5	3.2	62.6	30	3	7	9	11	12	14
	8	4	14.9	55.3	225	71	99	116	129	139	130
	9	3	25.5	46.0	281	137	176	198	214	223	184
	10	2	34.3	33.7	304	189	234	258	275	283	217
	11	1	40.4	18.2	314	221	270	295	312	320	236
	12		42.6	0.0	317	232	282	308	325	332	243
	Surface daily totals				2624	1474	1852	2058	2204	2286	1808

[a]From Kreider, J. F., and F. Kreith, "Solar Heating and Cooling," revised 1st ed., Hemisphere Publ. Corp., 1977.

[b]1 Btu/hr · ft^2 = 3.152 W/m^2. Ground reflection not included on normal or horizontal surfaces.

[c]Normal insolation does not include diffuse component.